

Potential Utilization of Specific Attenuation for Rainfall Estimation, Mitigation of Partial Beam Blockage, and Radar Networking

ALEXANDER RYZHKOV

*Cooperative Institute for Mesoscale Meteorological Studies, University of Oklahoma,
and NOAA/OAR/National Severe Storms Laboratory, Norman, Oklahoma*

MALTE DIEDERICH

Meteorological Institute, University Bonn, Bonn, Germany

PENGFEI ZHANG

*Cooperative Institute for Mesoscale Meteorological Studies, University of Oklahoma,
and NOAA/OAR/National Severe Storms Laboratory, Norman, Oklahoma*

CLEMENS SIMMER

Meteorological Institute, University Bonn, Bonn, Germany

(Manuscript received 19 February 2013, in final form 9 July 2013)

ABSTRACT

The potential utilization of specific attenuation A for rainfall estimation, mitigation of partial beam blockage, and radar networking is investigated. The $R(A)$ relation is less susceptible to the variability of drop size distributions than traditional rainfall algorithms based on radar reflectivity Z , differential reflectivity Z_{DR} , and specific differential phase K_{DP} in a wide range of rain intensity. Specific attenuation is estimated from the radial profile of the measured Z and the total span of the differential phase using the ZPHI method. Since the estimated A is immune to reflectivity biases caused by radar miscalibration, attenuation, partial beam blockage, and wet radomes, rain retrieval from $R(A)$ is also immune to the listed factors. The $R(A)$ method was tested at X band using data collected by closely located radars in Germany and at S band for polarimetrically upgraded Weather Surveillance Radar-1988 Doppler (WSR-88D) radars in the United States.

It is demonstrated that the two adjacent X-band radars—one of which is miscalibrated and another which is affected by partial beam blockage—produce almost indistinguishable fields of rain rate. It is also shown that the $R(A)$ method yields robust estimates of rain rates and rain totals at S band, where specific attenuation is vanishingly small. The X- and S-band estimates of rainfall obtained from $R(A)$ are in good agreement with gauges.

1. Introduction

Significant progress has been achieved in rainfall measurements after dual-polarization radars were introduced. The utilization of differential reflectivity Z_{DR} in combination with radar reflectivity Z helps to mitigate uncertainties related to the variability of drop size

distributions (DSD). Methods based on specific differential phase K_{DP} are less sensitive to DSD variations and are immune to attenuation and radar miscalibration. Biases in Z and Z_{DR} caused by attenuation, especially at shorter wavelengths, can be efficiently reduced using total differential phase Φ_{DP} . A typical solution for S band is a combination of an $R(K_{DP})$ relation for higher rain rates and an $R(Z, Z_{DR})$ relation for lower rain rates, where K_{DP} becomes noisy and increasingly susceptible to DSD variability (e.g., Giangrande and Ryzhkov 2008; Cifelli et al. 2011). At C and X bands, $R(K_{DP})$ is applied more extensively and for a larger range of rain intensities

Corresponding author address: Alexander Ryzhkov, CIMMS, University of Oklahoma, National Weather Center, 120 David L. Boren Blvd., Norman, OK 73072.
E-mail: alexander.ryzhkov@noaa.gov

than at S band, and it is usually complemented by an $R(Z)$ relation for lighter rain provided that Z is polarimetrically corrected for attenuation (Park et al. 2005; Figueras i Ventura et al. 2012; Vulpiani et al. 2012). The $R(Z, Z_{DR})$ relation is less efficient at shorter wavelengths because Z_{DR} can be strongly biased by differential attenuation, and the quality of its attenuation correction using differential phase is not sufficient to ensure the required accuracy of the Z_{DR} measurements within 0.1–0.2 dB if differential attenuation is significant.

Despite all the progress in polarimetric rainfall measurements, several practically important issues still remain to be addressed. Although the parameters of power-law type $R(K_{DP})$ relations are less sensitive to DSD variability than the parameters of $R(Z)$ relations, the utilization of a single $R(K_{DP})$ relation is not sufficient to capture the full range of DSD variability. Hence, $R(K_{DP})$ relations need to be optimized for particular DSD or rain regimes. Maps of instantaneous rain rates retrieved from $R(K_{DP})$ algorithms usually look much noisier and thus less appealing to the users than corresponding maps obtained using $R(Z)$ relations. Such noisiness may be visible even in the fields of hourly rain accumulation. Negative rain totals are occasionally retrieved, which may undermine the credibility of the algorithm. Moreover, the shape of smaller-size convective cells may be distorted in $R(K_{DP})$ maps because of difficulties in Φ_{DP} processing at smaller scales. Radial profiles of differential phase exhibit large-scale oscillations in areas of nonuniform beam filling, which reduces the magnitude of the cross-correlation coefficient ρ_{hv} and enhances perturbations of Φ_{DP} (Ryzhkov 2007). Despite recent attempts to improve Φ_{DP} processing (e.g., Wang and Chandrasekar 2009; Otto and Russchenberg 2011; Maesaka et al. 2012), reliable and robust routines for K_{DP} estimations do not exist at the moment. Careful separation of the contributions to Φ_{DP} from the K_{DP} -related forward-propagation effects and the backscatter differential phase δ is required at X band (e.g., Trömel et al. 2013). Thus, there is a need for a substitute for $R(K_{DP})$ when K_{DP} is corrupted and unreliable. Estimates of $R(Z)$ or $R(Z, Z_{DR})$ are obvious choices, but such estimates may suffer deficiencies due to miscalibration, partial blockage of the radar beam, uncompensated biases due to attenuation, and high sensitivity to DSD variability. There is not a single $R(Z, Z_{DR})$ relation that can be recommended for all rain types, a situation that is currently a challenge for polarimetrically upgraded Weather Surveillance Radar-1988 Doppler (WSR-88D) radars.

In view of all these problems, revisiting specific attenuation A as a possible radar variable for rainfall estimation and for a likely substitute for traditionally employed—but compromised— Z, Z_{DR} , and K_{DP} relations

is a natural undertaking. As opposed to Z , A is more directly related to rain rate and liquid water content, and its estimation may not be affected by radar miscalibration and blockage of the radar beam (depending on the method of its estimation). The low sensitivity of the $R(A)$ relation to DSD variability is well known and pointed out by Atlas and Ulbrich (1977) and Matrosov (2005).

The question is how to estimate attenuation. Using microwave links is one of the most direct methods (e.g., Moufouma 1984; Overeem et al. 2011). In the case of weather radar, this is a much greater challenge, and researchers were primarily interested in how to correct Z in the presence of attenuation rather than in measuring and capitalizing on A itself. A classical method for correcting Z for attenuation using a single-polarization radar was suggested by Hitschfeld and Bordan (1954). The Hitschfeld and Bordan algorithm was later refined using external constraints such as path-integrated attenuation (PIA), which should be estimated from an independent measurement (Meneghini and Nakamura 1990; Iguchi and Meneghini 1994; Marzoug and Amayenc 1994). In the case of dual-polarization radars, Bringi et al. (1990) and Testud et al. (2000) proposed utilizing the total span of the differential phase $\Delta\Phi_{DP}$ along the propagation path for estimating PIA as

$$\text{PIA} = \alpha\Delta\Phi_{DP} \quad (1)$$

(the “ZPHI method”; for details, see section 3). In Eq. (1), α is equal to the net ratio of A and K_{DP} along the ray. In fact, specific attenuation A is not used directly to estimate rain rate according to the ZPHI method. Instead, it is utilized as an interim parameter for calculating the normalized concentration of raindrops N_w (Testud et al. 2001), and the rain rate is computed from the combination of Z (corrected for attenuation) and N_w (Le Bouar et al. 2001).

In our study, we suggest utilizing A computed from the ZPHI formula for a direct estimation of rain rate. Because such an estimate of A is immune to radar miscalibration, partial beam blockage, and impacts of a wet radome, the corresponding $R(A)$ estimate is also insensitive to these factors. Moreover, there is no distortion of the shape of rain cells if the $R(A)$ relation is used. However, there are two major issues in determining A from ZPHI. One of them is the uncertainty of the $A(Z)$ relation due to the variability of N_w , and the other is the uncertainty in the ratio A/K_{DP} . The sensitivity of $R(A)$ estimates to these uncertainties is one of the issues examined in the paper. Once A is derived, the relation $R(A)$, although little sensitive to DSD variations, depends on temperature. This temperature dependency can,

however, be taken into account knowing the geometry of the beam and the vertical profile of temperature [currently easily available from numerical weather prediction (NWP) models]. The ZPHI method has never been utilized at S band [except in one conference paper by Le Bouar and Testud (2001)], which can be attributed to the fact that attenuation is small at S band. In this paper, we will show that the $R(A)$ method is even more promising at S band than at shorter radar wavelengths.

The $R(A)$ methodology has its advantages and disadvantages. One of the goals of this study is to show that it provides robust estimations of rainfall and that it can complement existing algorithms where they experience problems and where we anticipate A -based algorithms to work better despite all its limitations.

The paper is organized as follows. In section 2, the sensitivity of the $R(A)$ relations to the variability of drop size distributions is examined at different radar wavelengths. The procedure for the estimation of specific attenuation A is described in section 3 followed by sections 4–6, where the sensitivity of the A estimate to the radial variability of N_w , the uncertainty in the parameter α , and the presence of hail is evaluated. Section 7 contains application examples of the $R(A)$ methodology for rainfall estimation at X and S bands, and for radar networking.

2. Sensitivity of $R(A)$ relations to variability of drop size distributions at different radar wavelengths

A large DSD dataset collected during seven years of 2D video disdrometer measurements in Oklahoma is used to evaluate the sensitivity of the $R(A)$ relations at different radar wavelengths to the DSD variability. The details of the disdrometer measurements can be found in Schuur et al. (2001, 2005). The dataset contains 47144 DSDs encompassing a wide range of different rain types. Radar variables for each DSD have been simulated assuming the raindrop aspect ratio specified by Brandes et al. (2002) and a 10° width of the canting angle distribution. The optimal $R(Z)$, $R(K_{DP})$, and $R(A)$ power-law relations have been obtained using a standard weighted least squares polynomial fit. All rain rates associated with individual DSDs were separated into 30 intervals of $\log(R)$ with increments of 0.1 between -1.0 and 2.0 , and each interval was given a weight proportional to the total rain corresponding to this interval (i.e., mean rain rate of the interval multiplied by the number of DSDs belonging to it).

The $R(A)$ relation is much less sensitive to DSD variations than the $R(Z)$ and $R(K_{DP})$ algorithms. This is illustrated in Fig. 1, where the results of simulations are presented for S ($\lambda = 11.0\text{ cm}$), C ($\lambda = 5.3\text{ cm}$), and

X ($\lambda = 3.2\text{ cm}$) bands, and a temperature of 20°C . The advantage is most pronounced at S band, where specific attenuation A is very close to the 3.67th moment of the DSD (i.e., the one for rain rate). The $R(K_{DP})$ relation may exhibit lower sensitivity to DSD for very high rain rates at C and X bands, but $R(A)$ is less affected by DSD variability at lower rain rates. It is known that specific attenuation depends on temperature; hence, the parameters of $R(A)$ relations are temperature dependent as shown in Table 1, where the optimal power-law relations are listed at all three frequency bands for different temperatures and for horizontal and vertical polarization.

Although the temperature dependencies of intercept and exponent in the power-law relations are quite strong, they are easy to take into account knowing the vertical temperature profiles, which are widely available, for example, from the output of NWP models or soundings. It can be shown that a simple linear interpolation of intercepts and exponents in the $R(A)$ relations for the temperatures between 0° , 10° , 20° , and 30°C provides sufficient precision in rain-rate retrieval at an arbitrary temperature. Knowing the temperature with an accuracy of 5° results in errors lower than 10%–20% in rain-rate estimates. Note that using vertical polarization may be advantageous for implementing the $R(A)$ algorithm at C and X bands because the corresponding intercepts in the power-law relations are closer to 1; thus, the $R(A_v)$ relations are less sensitive to DSD variability than the $R(A_h)$ relations.

Specific attenuation strongly depends on radar wavelength. Therefore, the parameters of the $R(A)$ relation change significantly even within a particular band (S, C, or X). For the WSR-88D radars operating at S band, the intercept in the $R(A)$ relation increases by 35% as the radar wavelength changes from 10.0 to 11.0 cm . At S band, the dependencies of the intercept on temperature and radar wavelength can be approximated by the formula

$$R(A) = c_1(t)c_2(\lambda)A_h^{1.03}, \quad (2)$$

where

$$c_1(t) = (2.23 + 0.078t + 0.00085t^2)10^3 \quad (3)$$

$$c_2(\lambda) = 1 - 0.26(11.0 - \lambda). \quad (4)$$

In Eqs. (3) and (4), t is temperature ($^\circ\text{C}$) and λ is the radar wavelength (cm).

3. Estimation of specific attenuation A

Specific attenuation A can be computed from the radial profile of the attenuated reflectivity Z_a and the

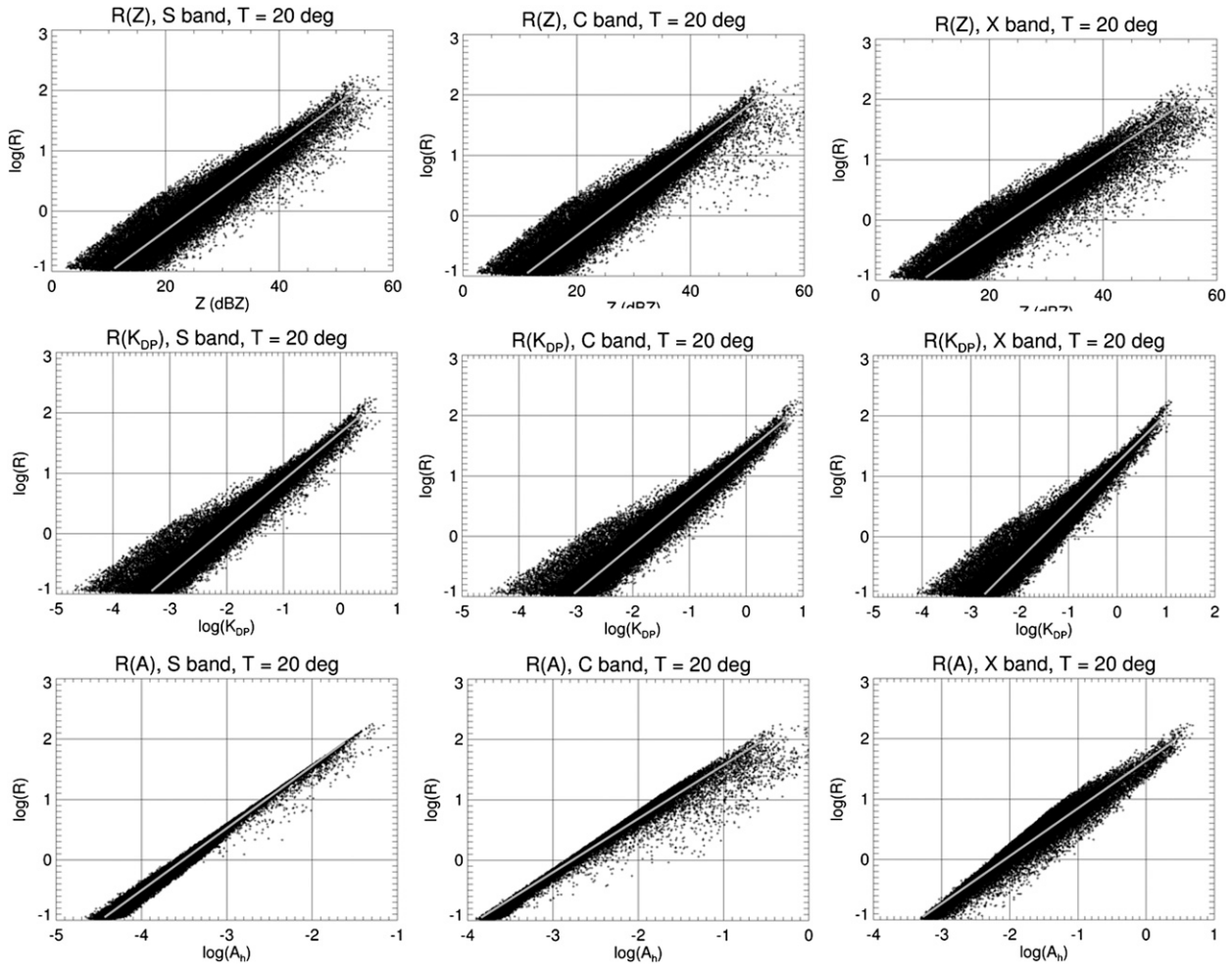


FIG. 1. Scatterplots of R vs Z , K_{DP} , and A at S ($\lambda = 11.0$ cm), C ($\lambda = 5.3$ cm), and X ($\lambda = 3.2$ cm) bands simulated from 47 144 DSDs measured in Oklahoma.

known two-way PIA along the propagation path (r_1, r_2) as (Meneghini and Nakamura 1990)

$$A(r) = \frac{a(r)[Z_a(r)]^b C(b, \text{PIA})}{I_a(r_1, r_2) + C(b, \text{PIA}) I_a(r, r_2)}, \quad (5)$$

where

$$I_a(r_1, r_2) = 0.46b \int_{r_1}^{r_2} a(s)[Z_a(s)]^b ds, \quad (6)$$

$$I_a(r, r_2) = 0.46b \int_r^{r_2} a(s)[Z_a(s)]^b ds, \quad (7)$$

$$C(b, \text{PIA}) = \exp(0.23b\text{PIA}) - 1. \quad (8)$$

In deriving (5) it is assumed that

$$A(r) = a(r)[Z(r)]^b, \quad (9)$$

where b is a constant parameter (usually within 0.6–0.9 at microwave frequencies) and Z is the intrinsic (not biased by attenuation) reflectivity factor expressed in linear scale. The factor a is directly related to the normalized concentration of raindrops N_w , which is defined by the liquid water content (LWC) and the mean volume diameter D_m of the drop size distribution (Testud et al. 2001):

$$a = c(T)N_w^{1-b}, \quad (10)$$

$$N_w = \frac{4^4 \text{ LWC}}{\pi \rho_w D_m^4}, \quad (11)$$

where $c(T)$ is a function of temperature and ρ_w is the density of water.

Equation (5) yields the *exact* solution for A provided that PIA and the radial dependency of a are known. If a is not a function of range, then Eq. (5) simplifies to

TABLE 1. Relations of $R(A)$ at different radar wavelengths, temperatures, and polarizations; R is expressed in mm h^{-1} , A is in dB km^{-1} .

Temp ($^{\circ}\text{C}$)	Horizontal polarization	Vertical polarization
X band ($\lambda = 3.2 \text{ cm}$)		
0	$R = 49.1 A_h^{0.87}$	$R = 57.8 A_v^{0.89}$
10	$R = 45.5 A_h^{0.83}$	$R = 53.3 A_v^{0.85}$
20	$R = 43.5 A_h^{0.79}$	$R = 51.1 A_v^{0.81}$
30	$R = 43.0 A_h^{0.76}$	$R = 51.0 A_v^{0.78}$
C band ($\lambda = 5.3 \text{ cm}$)		
0	$R = 221 A_h^{0.92}$	$R = 281 A_v^{0.95}$
10	$R = 250 A_h^{0.91}$	$R = 326 A_v^{0.94}$
20	$R = 294 A_h^{0.89}$	$R = 393 A_v^{0.93}$
30	$R = 352 A_h^{0.89}$	$R = 483 A_v^{0.93}$
S band ($\lambda = 11.0 \text{ cm}$)		
0	$R = 2.23 \times 10^3 A_h^{1.03}$	$R = 3.02 \times 10^3 A_v^{1.06}$
10	$R = 3.10 \times 10^3 A_h^{1.03}$	$R = 4.12 \times 10^3 A_v^{1.06}$
20	$R = 4.12 \times 10^3 A_h^{1.03}$	$R = 5.51 \times 10^3 A_v^{1.06}$
30	$R = 5.33 \times 10^3 A_h^{1.03}$	$R = 7.19 \times 10^3 A_v^{1.06}$

$$A(r) = \frac{[Z_a(r)]^b C(b, \text{PIA})}{I(r_1, r_2) + C(b, \text{PIA}) I(r, r_2)}, \quad (12)$$

where

$$I(r_1, r_2) = 0.46b \int_{r_1}^{r_2} [Z_a(s)]^b ds \quad (13)$$

and

$$I(r, r_2) = 0.46b \int_r^{r_2} [Z_a(s)]^b ds. \quad (14)$$

Bringi et al. (1990) suggested estimating PIA using differential phase Φ_{DP} as

$$\text{PIA}(r_1, r_2) = \alpha[\Phi_{\text{DP}}(r_2) - \Phi_{\text{DP}}(r_1)] = \alpha\Delta\Phi_{\text{DP}}, \quad (15)$$

and Testud et al. (2000) and LeBouar et al. (2001) utilized Eqs. (12) and (15) to obtain radial profiles of specific attenuation A at C band. To account for the variability of a in Eq. (9), they divide the propagation path into the segments where Φ_{DP} changes by 6° and assume that a (or N_w) is constant within each individual segment so that Eq. (12) can be utilized safely. In each segment, the values of N_w are determined from Eqs. (9) and (12) using the estimated A and Z corrected for attenuation from the results of the A estimation in neighboring segments closer to the radar. The rain rate is then calculated from an $R(Z, N_w)$ relation that is very robust with respect to DSD variability. The described methodology is referred to as the ZPHI method. Its most recent version is described by Tabary et al. (2011).

The need for ray segmentation and the vulnerability to radar reflectivity biases caused by possible radar

miscalibration, partial beam blockage, and wet radome are the weaknesses of the ZPHI method. The essence of our approach is 1) to avoid excessive segmentation of the radar ray either by not using segmentation at all or by dividing the ray into a small number (ideally two) of large segments with reliably measured $\Delta\Phi_{\text{DP}}$ and 2) to estimate rain rate directly from specific attenuation A computed from (12). The approach is both simple and immune to Z biases caused by radar miscalibration, wet radome, partial beam blockage, and inadequate correction for attenuation. Rain-rate fields estimated from $R(A)$ have the same spatial resolution and structure as $R(Z)$, whereas the shapes of rain cells retrieved by $R(K_{\text{DP}})$ are commonly distorted and the fields of $R(K_{\text{DP}})$ are much noisier, particularly at lower rain rates.

4. Impact of radial variability of N_w

As opposed to ZPHI, the radial variability of N_w is neglected in the $R(A)$ method unless a real “hot spot” (such as hail) is found along the propagation path in rain. We believe that in the overwhelming majority of situations, this assumption results in tolerable errors in retrieved A , which are outweighed by the advantages of the technique.

Testud et al. (2000) examined the impact of the radial variability of N_w by simulating two artificial rain cells with significantly different N_w . In our study, we use real radar data collected in various storms with strong radial nonuniformity to retrieve actual radial profiles of N_w using well-calibrated Z and Z_{DR} observations. The method for the N_w retrieval is similar to the “integrated ZZDR algorithm” by Illingworth and Thompson (2005) also described in Tabary et al. (2011). Data from three storms that produced heavy rain and were observed by three polarimetrically upgraded S-band WSR-88D radars are used in the simulations. One of the storms was observed with the KOUN WSR-88D radar and produced a flash flood in Oklahoma City (OKC), Oklahoma, on 14 June 2010. Another one was associated with Hurricane Irene on 27 August 2011 and caused massive flash floods along the U.S. East Coast. The third storm (20 May 2011) represents a mesoscale convective system typical for the U.S. Great Plains.

Typical fields of $\log(N_w)$ for the three storms are represented in Fig. 2 together with the corresponding Z maps. The color coding covers a range in $\log(N_w)$ from less than 2.625 (index 0) to larger than 4.375 (index 7), where N_w is expressed in cubic meter per millimeter ($\text{m}^{-3} \text{ mm}^{-1}$). Low values of $\log(N_w)$ represent “continental rain” characterized by low concentrations of large raindrops, whereas high values of $\log(N_w)$ correspond to “tropical rain” with high concentrations of smaller raindrops (Bringi et al. 2003). Figure 2 shows that the

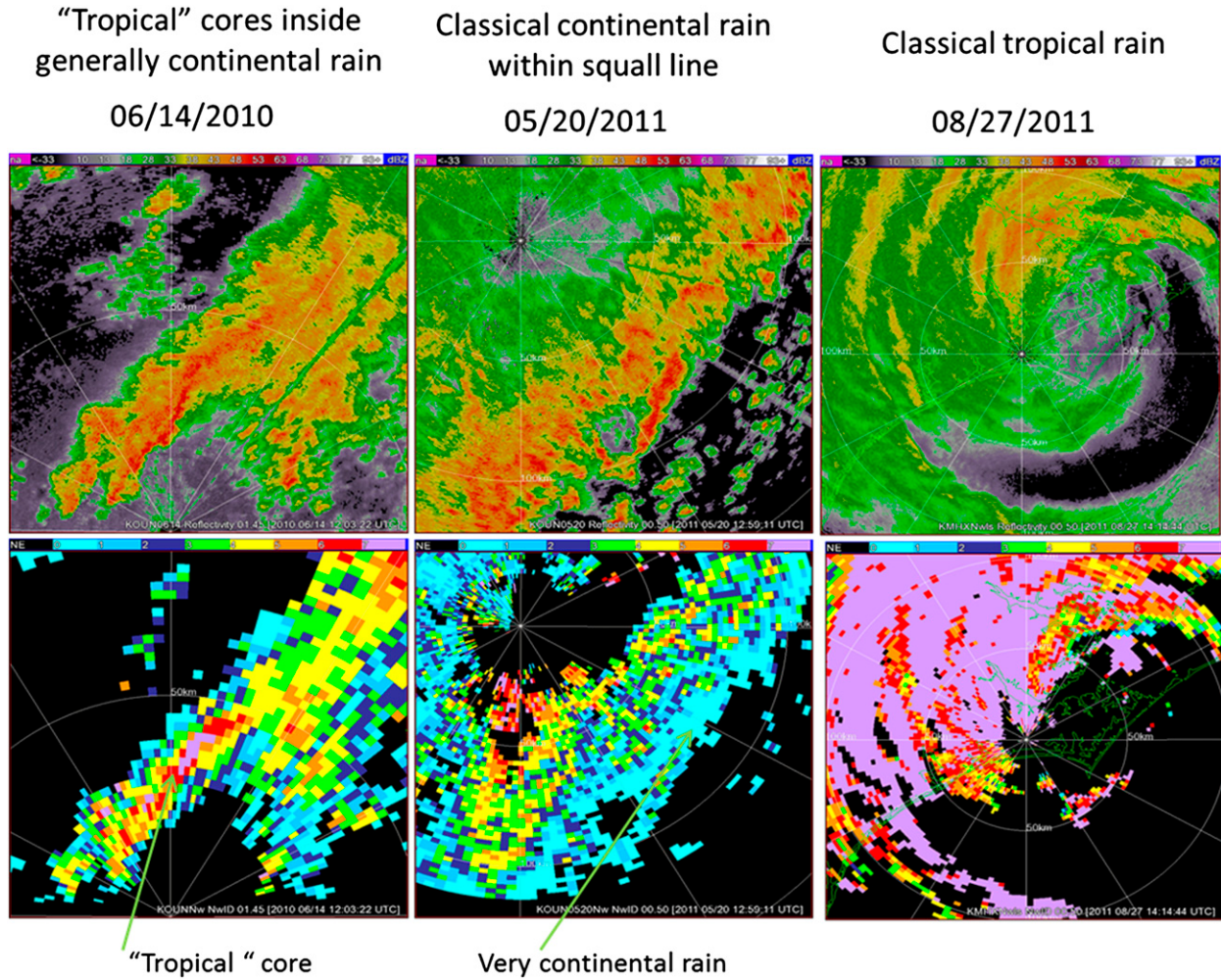


FIG. 2. Examples of PPIs of Z and $\log(N_w)$ for three storms producing heavy rain observed with three different polarimetric WSR-88D radars. The color coding in the bottom panels covers a range in $\log(N_w)$ from less than 2.625 (index 0) to larger than 4.375 (index 7). Low values of $\log(N_w)$ represent continental rain characterized by low concentrations of large raindrops, whereas high values of $\log(N_w)$ correspond to tropical rain with high concentrations of smaller raindrops; N_w is expressed in $\text{m}^{-3} \text{mm}^{-1}$.

lowest values of $\log(N_w)$ are found in the squall line on 20 May 2011, which represents typical continental rain. The values of N_w are almost two orders of magnitude higher for Hurricane Irene. It is interesting that the case of the OKC flash flood on 14 June 2010 exhibits features of both continental and tropical rain with cores of “tropical” rain immersed within “continental” rain.

After N_w is determined, the ratio $x = \log(Z/N_w)$ is utilized to estimate $y = \log(A/N_w)$ using the formula

$$y = a_0 + a_1 x + a_2 x^2 + a_3 x^3, \quad (16)$$

where

$$\begin{aligned} a_0 &= -6.12 - 0.012t, & a_1 &= 0.622 - 0.0002t, \\ a_2 &= 0.0250, & a_3 &= 0.00424 \end{aligned}$$

at S band and t is temperature ($^{\circ}\text{C}$). Equation (16) is derived from simulations based on a large DSD dataset obtained in Oklahoma. Temperature for a given range gate is determined using the distance from the radar and the elevation angle assuming a linear vertical profile of temperature with a lapse rate of $6.5^{\circ} \text{ km}^{-1}$. Then the value of specific attenuation A at S band is obtained from y and N_w , which is considered as the “true” value of A at S band in the storm. Formulas similar to (16) are used to simulate the corresponding fields of A at C and X bands, which would be observed in the same storm assuming that $\log(Z/N_w)$ does not depend on radar wavelength.

As an example, we took the radial of S-band data collected at 1202 UTC 14 June 2010 at azimuth angle 14.2° , which cuts through a core of tropical rain. The

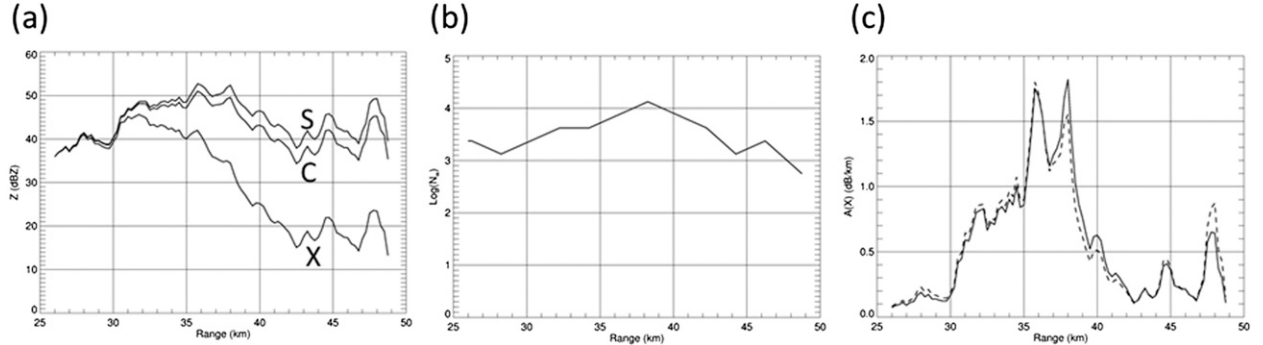


FIG. 3. Radial profiles of (a) attenuated Z at S (observed), C (computed), and X bands (computed); (b) retrieved $\log(N_w)$; and (c) true (solid line) and estimated (dashed line) specific attenuation A at X band. The data in the plots have been simulated from Z and Z_{DR} observed by the KOUN WSR-88D radar in central Oklahoma during a flash flood event in Oklahoma City at 1202 UTC 14 Jun 2010 (azimuth 14.2°). The term N_w is expressed in $\text{m}^{-3} \text{mm}^{-1}$.

measured radial profile of S-band Z is presented in Fig. 3a along with the corresponding simulated profiles at C and X bands. The retrieved radial profile of $\log(N_w)$ is displayed in Fig. 3b. Within the range interval between 25 and 50 km from the radar, the two-way path-integrated attenuation at S, C, and X bands is 0.4, 4, and 24 dB, respectively. The term N_w changes by more than an order of magnitude in this range interval. Figure 3c shows the profile of the true simulated A at X band (solid line) and its estimate (dashed line) using the approximate solution [Eq. (12)], implying that the factors N_w and a in the $A(Z)$ relation are constant within the examined range interval. Surprisingly, the difference between the true and estimated profiles of A is quite small.

We performed a statistical analysis of the errors in the A retrieval using Eq. (12) by examining a large number of radials for the three selected storms and found that the estimated A has only small biases, and that the standard fractional error decreases from about 40% at rain rates of 2 mm h^{-1} to 10% for rain rates of 80 mm h^{-1} at S, C, and X bands. An example of a scatterplot of true A versus its estimate at S band for the whole plan position indicator (PPI) of the radar data collected during Hurricane Irene (rightmost panels in Fig. 2) is presented in Fig. 4. The examples shown and the statistical analysis demonstrate that the true radial profiles of A are quite well approximated by its estimate from Eq. (12) even in the most challenging cases of convective heavy rain with significant DSD variability characterized by N_w ; the errors are in the range of about 20%. It has to be emphasized that the retrieval routine works if only rain is present along the propagation path. If hail is present in any part of the propagation path, then the A retrieval may fail along the whole propagation path, and not only in the location of hail, due to the integral nature of Eq. (12). In such a case, the areas of hail should be

identified, and the method has to be applied separately to the portions of the propagation path between the radar and the hail cell and behind the hail (see sections 6 and 7).

5. The errors caused by uncertainty of the factor α

While nonuniformity of N_w along the propagation path causes relatively minor and generally acceptable errors (if hail is isolated), the uncertainty of the factor α in (15) produces much larger errors in the estimation of the radial profile of N_w . The factor α , which is equal to

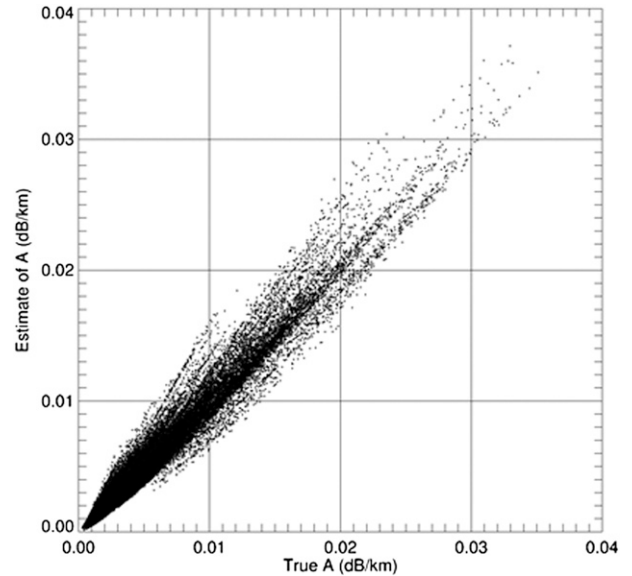


FIG. 4. Scatterplot of true A estimated from the measured Z and Z_{DR} at the 0.5° elevation sweep for Hurricane Irene (right panels in Fig. 1) by the KMHX WSR-88D radar vs its estimate using Eq. (12).

the net ratio of A to K_{DP} along the ray, depends on temperature and is prone to DSD variability. The scatterplots of α versus differential reflectivity Z_{DR} (as a proxy for DSD variability) in the three radar frequency bands for 0° and 30°C are displayed in Fig. 5. Both temperature- and DSD-related variations of α are significant.

Decreasing the ratio α by a factor of 2 dramatically affects the retrieved radial profiles of A at all three radar wavelengths as Fig. 6 shows. At S band, the retrieved A is reduced approximately twice uniformly along the ray, whereas the biases at C and X bands can be much larger or smaller depending on the range. For small PIA, the factor $C(b, \text{PIA})$ in Eq. (8) can be expanded as

$$\begin{aligned} C(b, \text{PIA}) &= \exp(0.23b\text{PIA}) - 1 \approx 0.23b\text{PIA} \\ &= 0.23b\alpha\Delta\Phi_{DP}(r_1, r_2) \end{aligned} \quad (17)$$

and specific attenuation A retrieved from Eq. (12) is approximately linearly dependent on α . This is most often the case at S band but not at C or X band.

The uncertainty of α is not a specific issue of the $R(A)$ method but pertains to all polarimetric techniques for attenuation correction that utilize Eq. (15). There are several possible approaches to estimate the value of α along the propagation path. One of them is the method of Bringi et al. (2001), which attempts to optimize α by minimizing the difference between the measured profile of Φ_{DP} along the ray and the estimated Φ_{DP} from the retrieved profile of A . The method produces mixed results, but there is no other accepted alternative at the moment. Another possible approach is to estimate PIA from noise measurements, that is, by using the radar as a radiometer (Fabry 2001; Illingworth et al. 2011). The net parameter α can then be estimated as the ratio of PIA and $\Delta\Phi_{DP}$. This may be a promising technique, but it requires an exploratory study.

At shorter radar wavelengths, the ratio $\alpha = A/K_{DP}$ can be roughly estimated from the ratio $\beta = A_{DP}/K_{DP}$ (where A_{DP} is specific differential attenuation), which is easier to evaluate from the data than the parameter α if differential attenuation is sufficiently strong. In this case, $\beta = |\Delta Z_{DR}|/\Delta\Phi_{DP}$, where ΔZ_{DR} is the negative bias of Z_{DR} caused by differential attenuation. The coefficient of proportionality γ between α and β ($\beta = \gamma\alpha$) may vary depending on the DSD, but this dependence appears not be too strong at X band. Table 2 contains median values of γ at S, C, and X bands computed from the simulations based on the Oklahoma DSD dataset for very continental [$\log(N_w) < 2.5$] and very tropical [$\log(N_w) > 4.2$] rain at $T = 20^{\circ}\text{C}$ and $Z > 40 \text{ dBZ}$, where attenuation is most significant. The dependence of γ on rain type is much stronger at S and C bands than at X band, where the suggested approach might work best.

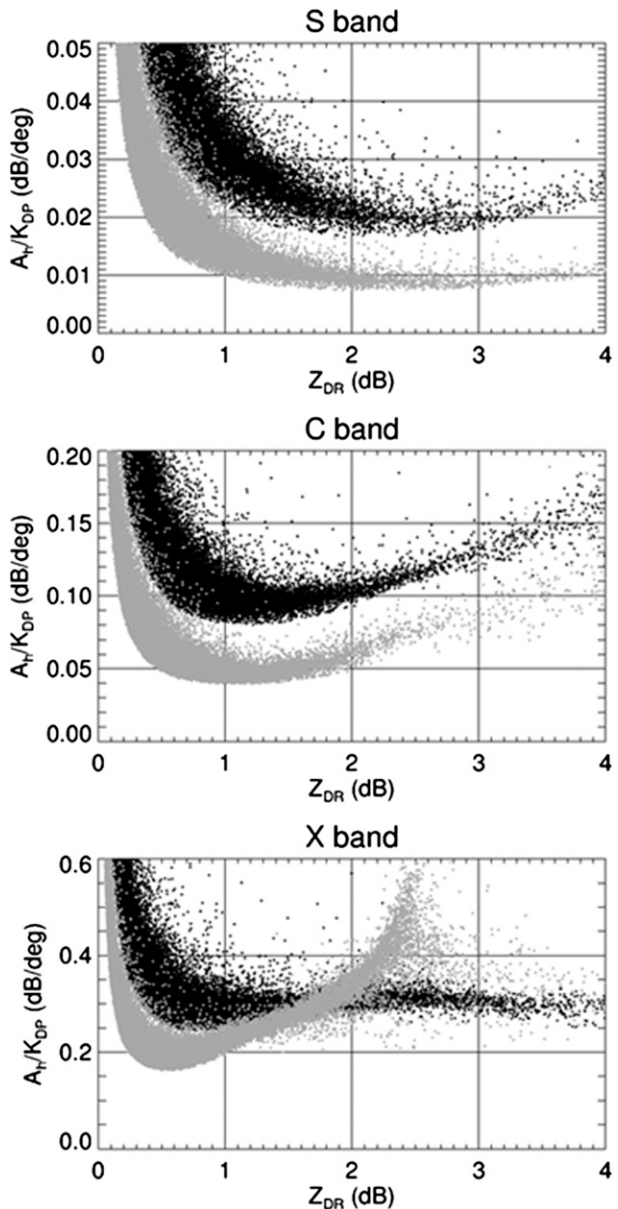


FIG. 5. Scatterplot of $\alpha = A/K_{DP}$ vs Z_{DR} at S ($\lambda = 11.0 \text{ cm}$), C ($\lambda = 5.3 \text{ cm}$), and X ($\lambda = 3.2 \text{ cm}$) bands simulated at two temperatures: 0°C (black dots) and 30°C (gray dots) using 47 144 DSDs measured in Oklahoma.

At longer wavelengths (S band), we suggest the routine based on PIA estimation using the radial profile of A retrieved from well-calibrated measurements of Z and Z_{DR} as described in section 4. This would require very accurate estimates of Z and Z_{DR} (with 1 dB and 0.1 dB precision, correspondingly). The routine has better chances to work for S band because both Z and Z_{DR} are least affected by attenuation. Because of the strong sensitivity of the N_w retrieval to errors in Z and Z_{DR} , the estimate of A using Eq. (16) is much less reliable than

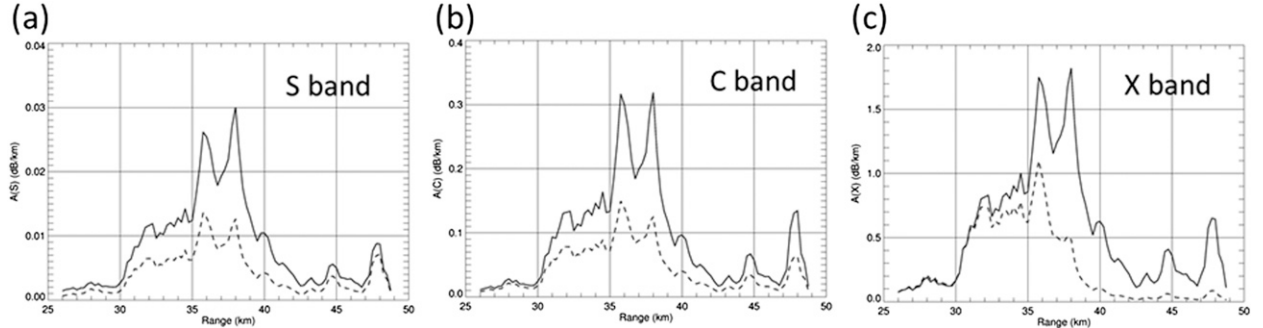


FIG. 6. Comparison of the true radial profiles of A at (a) S, (b) C, and (c) X bands (solid lines) with their estimates if the parameter α is reduced twice (dashed lines) for the radial of data illustrated in Fig. 2.

the one obtained from Eq. (12), which depends only on measurements of differential phase, which are immune to the factors affecting the quality of Z and Z_{DR} . Hence, Eq. (16) can be used only for relatively crude independent estimates of PIA or α . Our analysis shows that the value of α obtained using the described procedure may change noticeably from ray to ray, but it is possible to characterize the dominant type of rain and thus its “net” value of α quite adequately. For example, the estimated α varies from 0.02 to 0.03 dB deg $^{-1}$ over most areas of Hurricane Irene and is within 0.008–0.015 dB deg $^{-1}$ for the OKC flash flood case on 14 June 2010. This reflects the profound microphysical difference between both storms.

6. The performance of the $R(A)$ method in the presence of hail

The retrieval of specific attenuation A based on Eq. (12) may fail in “hot spots” where the factor $a(r)$ in Eq. (9) changes dramatically (like in the presence of hail). This would adversely affect the quality of the A estimate not only within the hot spot but everywhere along the ray due to the integral nature of the ZPHI algorithm. To illustrate this effect, we simulate the performance of the $R(A)$ algorithm for S band in the presence of a typical hot spot, namely, a strong hail cell along the propagation path.

Intrinsic (nonattenuated) values of Z , A , K_{DP} , and rain-rate R are modeled for a core of melting hail surrounded by heavy and moderate rain using the results of theoretical studies by Ryzhkov et al. (2009, 2012). The hail cell is assumed to be axisymmetric with a radius of 10 km. Radial profiles of Z , A , K_{DP} , and R through the convective cell are displayed in Fig. 7. The inner-core region with a radius of 2 km and reflectivities approaching 70 dBZ contains large hail particles with maximal diameters D_{max} of 35 mm. This core region is embedded in an area of moderate-size hail ($Z = 58.7$ dBZ,

$D_{\text{max}} = 24$ mm) extending to a radius of 3 km that in turn is embedded in an area of small hail ($Z = 54.0$ dBZ, $D_{\text{max}} = 14$ mm) up to a radius of 5 km. Heavy rain without hail ($Z = 52.0$ dBZ) surrounds this hail core up to a radius of 10 km (range segments from 15 to 20 and from 30 to 35 km). The whole convective cell is immersed in moderate rain of 10 mm h $^{-1}$ and Z of about 40 dBZ. The maximal rain rate in the middle of the hail core is 125 mm h $^{-1}$.

The attenuated reflectivity factor is obtained using the radial dependencies of intrinsic Z and A shown in Fig. 7. PIA within the range interval from 0 to 50 km is calculated using values of $\alpha = 0.015$ dB deg $^{-1}$, $b = 0.62$, while the magnitude of $\Delta\Phi_{\text{DP}} = 88.5^\circ$ is computed via integration of the radial profile of K_{DP} shown in Fig. 7. The radial dependencies of radar-derived rain rates using the three rainfall relations

$$R(Z) = 1.7010^{-2} Z^{0.714}, \quad (18)$$

$$R(K_{\text{DP}}) = 44.0 K_{\text{DP}}^{0.822}, \quad (19)$$

and

$$R(A) = 4.12 \times 10^{-3} A^{1.03} \quad (20)$$

are compared with the true radial profile of rain rate in Fig. 8. It is not surprising that the Next Generation Weather Radar (NEXRAD) $R(Z)$ relation grossly overestimates the rain rate everywhere along the propagation path (dashed line). The $R(A)$ relation produces a large

TABLE 2. Median ratios $\gamma = \beta/\alpha$ for continental and tropical rain at S, C, and X bands ($T = 20^\circ\text{C}$) obtained from simulations based on 47 144 DSD measurements in Oklahoma.

Rain type	$\gamma(S)$	$\gamma(C)$	$\gamma(X)$
Continental [$\log(N_w) < 2.5$]	0.36	0.39	0.19
Tropical [$\log(N_w) > 4.2$]	0.12	0.14	0.14

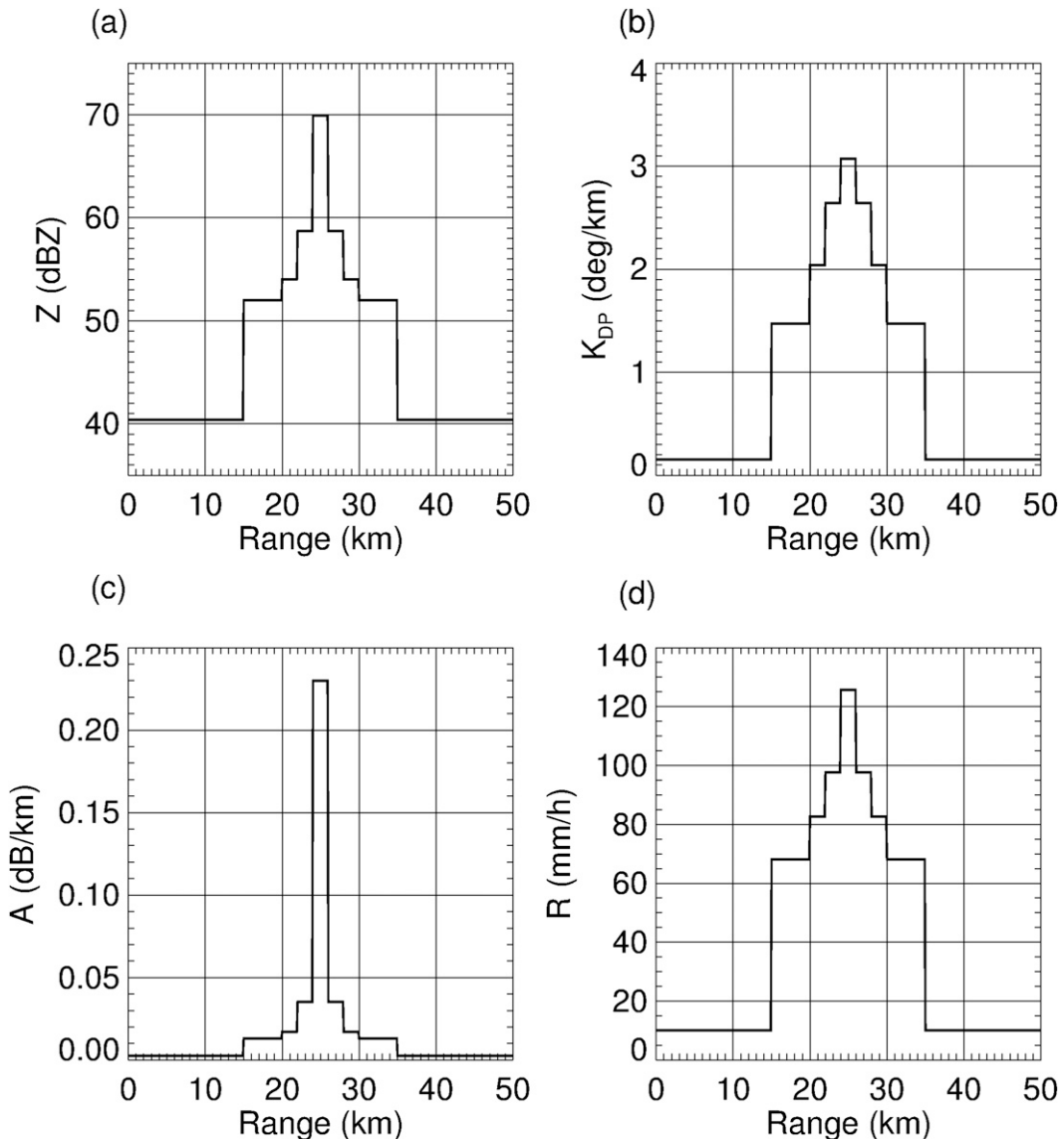


FIG. 7. Model radial distributions of S-band (a) Z , (b) K_{DP} , and (c) A as well as (d) R through a convective cell containing hail (Ryzhkov et al. 2012).

positive bias in the areas of large- and moderate-size hail but underestimates rain in the presence of smaller hail and the surrounding rain (moderate and heavy). Since the presence of a small segment of large hail within the ray can spoil the $R(A)$ estimate along the whole ray, it is necessary to identify hail and apply the method separately to the portions of the propagation path between the radar and hail cell and behind hail cell. Such a procedure is illustrated in section 7.

Figure 8 shows that the $R(K_{DP})$ relation [Eq. (19)] works best in the presence of hail as expected although with a slight underestimation of rain that progresses with increasing hail size, as mentioned in Ryzhkov et al. (2012).

7. Examples of $R(A)$ applications at X and S bands

a. $R(A)$ at X band

The $R(A)$ method was first tested at X band using the data collected by the X-band polarimetric radar at the University of Bonn (BoXPol) and a similar radar close to Juelich (JuXPol), 45 km northwest of the Bonn radar, for a moderate-to-heavy rain event on 22 June 2011. The BoXPol radar experiences significant beam blockage in the southern sector at the lowest antenna elevation (El) of 0.5° . This blockage is still noticeable at $El = 1.5^\circ$ with a narrow sector of substantial blockage in the southeast sector, where radar reflectivity is biased by -10 to -15 dBZ.

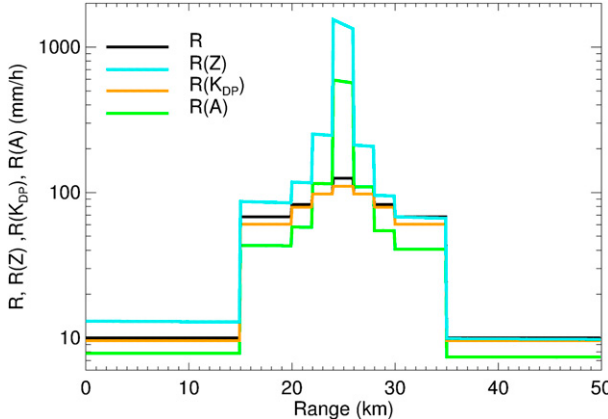


FIG. 8. Radial profiles of the true rain rate through the hail-bearing convective cell of Fig. 7 (black line) and its estimates based on $R(Z)$ (blue line), $R(K_{DP})$ (red line), and $R(A)$ (green line) at S band.

This negative Z bias causes a tremendous rain-rate underestimation in the partially blocked sector after Z is converted to R according to the standard Marshall–Palmer relation commonly used in this part of Germany, defined as

$$R(Z) = 0.029Z^{0.67} \quad (21)$$

(Fig. 9a). At 1125 UTC, a line of heavy rain east of the radar produces significant attenuation of the radar signal, resulting in large Z biases if Z is not corrected for attenuation. A simple linear correction of Z using the relation $\Delta Z = 0.27\Phi_{DP}$ restores the intrinsic radar reflectivity in the eastern sector and improves the $R(Z)$ estimates there (Fig. 9b). However, a blank southeastern sector still remains after the linear attenuation correction is applied because a correction for partial beam blockage (PBB) was not made.

Estimates of differential phase Φ_{DP} and specific differential phase K_{DP} are immune to PBB; hence, the field of rain rate estimated from the $R(K_{DP})$ relation

$$R(K_{DP}) = 16.9|K_{DP}|^{0.801}\text{sign}(K_{DP}) \quad (22)$$

does not show a blank southeastern sector but exhibits enhanced noisiness in areas of lighter rain (Fig. 9c). The $R(A)$ estimate assuming a temperature of 20°C (Table 1),

$$R(A) = 43.5A^{0.79}, \quad (23)$$

is also immune to PBB but shows in addition a good consistency with the $R(Z)$ field in terms of structure at all rain rates as opposed to the $R(K_{DP})$ field (see Fig. 9d).

The fields of rain rates retrieved from BoXPol are compared with the corresponding fields estimated from

JuXPol at about the same time (Figs. 9e–g) at elevation 1.1°. JueXPol was apparently miscalibrated at that time, and the radar reflectivity factor was negatively biased as the comparison of Figs. 9a and 9b with Figs. 9e and 9f indicates.

Since K_{DP} is not affected by radar miscalibration, the fields of $R(K_{DP})$ obtained by both radars are consistent in the areas of heavier rain along the squall line but are very noisy and erratic elsewhere (Figs. 9c,g). In contrast, rain-rate fields estimated from both radars using the $R(A)$ relation match each other very well at all rain intensities everywhere in the analyzed area (Figs. 9d,h). Remarkably, both radars, one of which is significantly miscalibrated and another one experiencing significant partial beam blockage, are capable of producing almost indistinguishable instantaneous rain-rate fields in the presence of significant attenuation if the $R(A)$ method is used. This shows great promise for utilizing the suggested technique for networking and compositing data from different radars, particularly in locations with rugged terrain. No digital elevation map information was required to eliminate the impact of PBB in this example.

A closer look at the sector where PBB occurs and where rain is of moderate or high intensity (Fig. 10) demonstrates that the $R(K_{DP})$ estimate of instantaneous rain rate from the perspective of the Bonn X-band radar is noisier than the $R(A)$ estimate, which is more consistent with $R(Z)$ in terms of texture and structure. Radial profiles of $R(Z)$ (after Z is corrected for attenuation), $R(K_{DP})$, and $R(A)$ along the direction marked by a line in Fig. 10 ($Az = 148^\circ$) are displayed in Fig. 11. It is evident that the shape of small convective rain cells is distorted if retrieved via K_{DP} . Indeed, the maxima of $R(K_{DP})$ may be shifted from the maxima of $R(Z)$, and positive and negative oscillations of $R(K_{DP})$ are evident toward the end of the radial. On the other hand, the shape of rain cells obtained from $R(A)$ perfectly matches the one retrieved from $R(Z)$.

Five months of continuous $R(A)$ estimates from BoXPol were compared with observations from 133 rain gauges within a 60-km distance from the radar. Equation (23) was used along the ray if Φ_{DP} exceeded 4° and the $R(Z)$ relation (21) was utilized otherwise after Z was corrected for attenuation and PBB. The biases, rms errors, and correlation coefficients for hourly rain totals are shown as functions of the distance from the radar in Fig. 12 (bottom panels). These are contrasted with the corresponding metrics for the $R(K_{DP})$ estimator [Eq. (22)] (top panels in Fig. 12). The $R(A, Z)$ rainfall estimator clearly outperforms the $R(K_{DP})$ relation (the favorite choice estimator at X band nowadays) at the ranges up to 60 km from the radar.

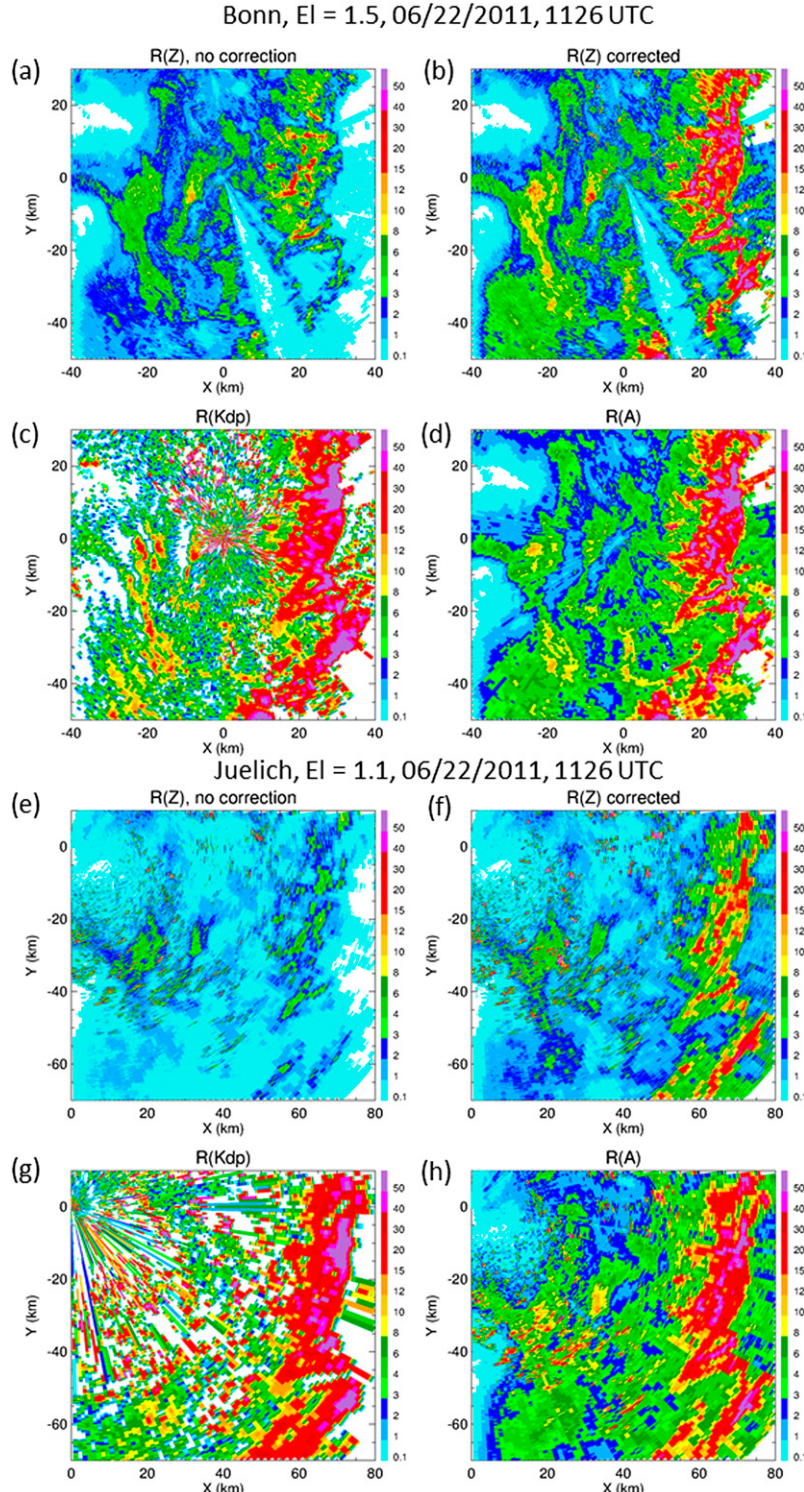


FIG. 9. Fields of rain rates retrieved from the Bonn and Juelich X-band radars using different rainfall algorithms at 1125–1126 UTC 22 Jun 2011: (a),(e) $R(Z)$ estimates before correction of Z for attenuation; (b),(f) $R(Z)$ estimates after Z correction; (c),(g) $R(K_{DP})$ estimates; and (d),(h) $R(A_h)$ estimates. The Bonn data are collected at elevation 1.5°, whereas the Juelich data are from elevation 1.1°. The Bonn and Juelich radars are located at $X = 0$ km, $Y = 0$ km in the top four and bottom four panels, respectively.

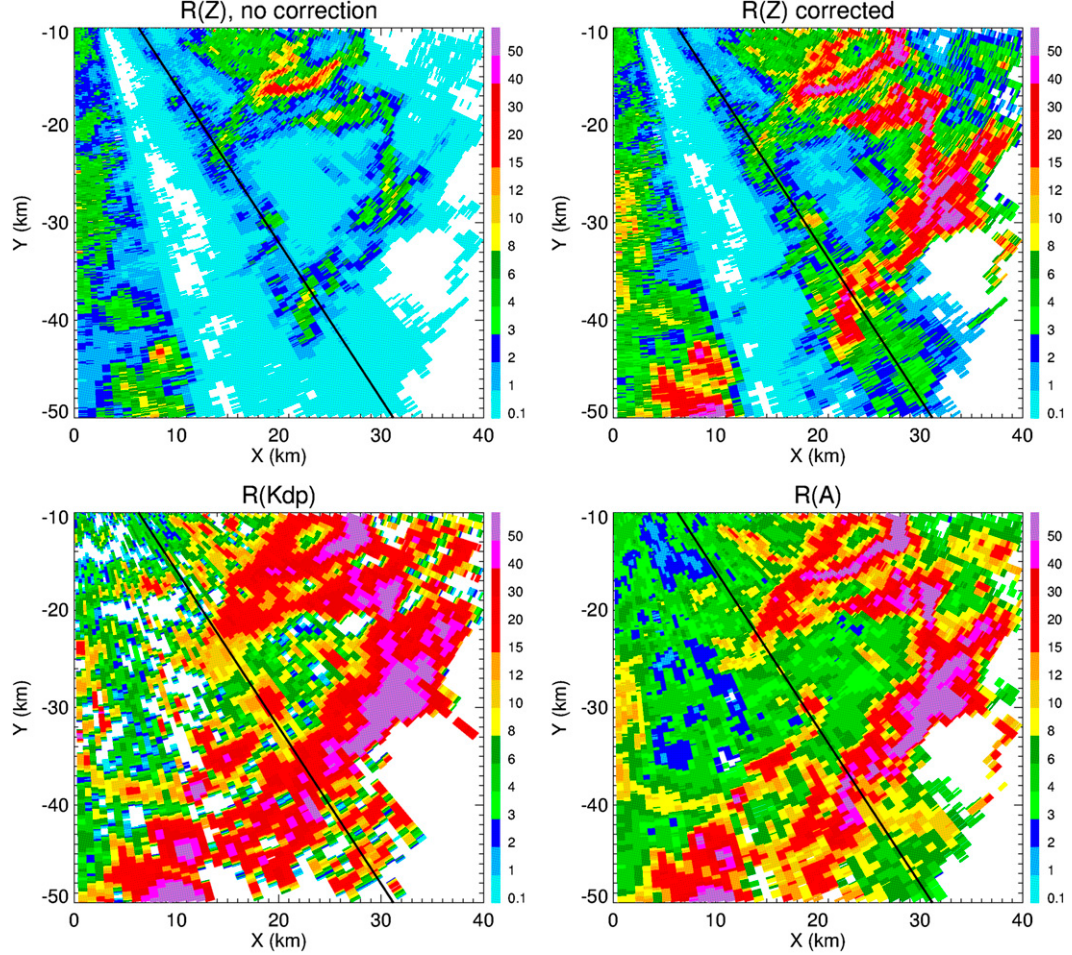


FIG. 10. Fields of $R(Z)$ (before and after attenuation correction), $R(K_{DP})$, and $R(A)$ in the area southeast from the Bonn radar (see Fig. 9). Solid line indicates $Az = 148^\circ$.

b. $R(A)$ at S band

Equation (12) and the ZPHI method were first applied at C band (Testud et al. 2000) and later at X band, where attenuation of microwave radiation in precipitation is significant. Le Bouar and Testud (2001) mentioned that it can be utilized at S band as well, but the overall perception was that A -based algorithms are not promising at longer wavelengths because specific attenuation is vanishingly small. It is interesting that the basic Eq. (12) does not show any contraindications for its use at S band provided that $\Delta\Phi_{DP}$ is large enough (at least more than 2° – 3°). We tested the $R(A)$ algorithm at S band for several cases with moderate-to-heavy precipitation, including the ones that are illustrated in Fig. 2.

The fields of Z , $R(Z)$, and $R(A)$ estimated from the KVNX WSR-88D radar at elevation 0.5° at 0916 UTC 20 May 2011 are displayed in Fig. 13. The $R(A)$ equation

$$R(A) = 4.12 \times 10^3 A^{1.03} \quad (24)$$

and $\alpha = 0.015 \text{ dB deg}^{-1}$ were used to estimate rain rate. Notable is the partial blockage of the radar beam in the western sector, which results in an underestimation of Z and rain rates computed from Z . The bias caused by blockage is completely eliminated in the $R(A)$ -derived field. Again, no digital elevation information was utilized to remove the blockage impact. The texture of the $R(A)$ map is totally consistent with the texture of the $R(Z)$ map for instantaneous rain rates. The differences between small-scale textures of the fields of $R(Z)$, $R(K_{DP})$, and $R(A)$ are better represented in Fig. 14, where a smaller area is displayed for the same case. The retrieved rain rates are shown only for pixels where $Z > 45 \text{ dBZ}$ and where the K_{DP} -based estimate of R can be potentially used at S band, assuming that the inherent noisiness of K_{DP} is not too high. The $R(A)$ algorithm retains the same radial resolution as $R(Z)$ (i.e., 0.25 km).

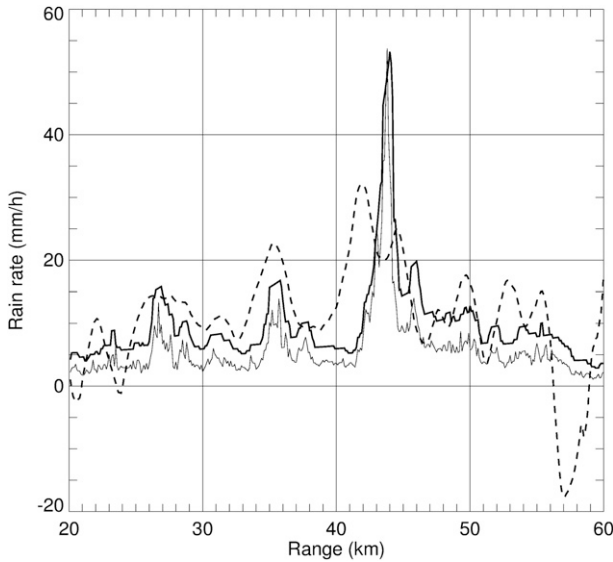


FIG. 11. Radial profiles of $R(Z)$ after correction for attenuation (thin solid line), $R(K_{DP})$ (dashed line), and $R(A)$ (thick solid line) at $Az = 148^\circ$ along the line shown in Fig. 10.

According to the WSR-88D radar processing algorithm, the radial resolution of the $R(K_{DP})$ estimate is 2 km at $Z > 40 \text{ dBZ}$, which is 8 times lower than the radial resolution of the $R(Z)$ and $R(A)$ estimates. Moreover, small-scale rain structures might be distorted, and negative rain rates do appear in the $R(K_{DP})$ map.

The maps of 6-h rain totals computed for the period 0800–1400 UTC 20 May 2011 using the $R(Z)$ and $R(A)$ algorithms are shown in Fig. 15. Again, the blockage impact is completely wiped out in the rain accumulation retrieved by the $R(A)$ technique. Moreover, the $R(A)$ algorithm yields better or similar quality rain accumulation estimates as compared to the standard $R(Z)$ relation in the areas free of blockage as the comparison with gauges indicates (Fig. 16).

Similar comparisons with gauges at S band have been made for another three events with heavy rain. These have been observed by the KTLX WSR-88D radar in the Oklahoma City metropolitan area on 14 June 2010, by the KMHX WSR-88D radar during Hurricane Irene on 26–28 August 2011, and by the KDLH WSR-88D radar in Duluth, Minnesota, on 30 June 2012. Two of these storms are illustrated in Fig. 2. The scatterplots of rain totals estimated using relation Eq. (24) versus their gauge estimates for the three rain events are displayed in Fig. 17. The corresponding bias ratios, fractional rms errors (FRMSEs), and correlation coefficients are listed in Table 3. It is remarkable that a single relation (24) with a fixed parameter $\alpha = 0.015 \text{ dB deg}^{-1}$ yields high-quality estimates of rainfall for all events. Only Hurricane Irene requires an adjustment of the factor α (using $\alpha = 0.025 \text{ dB deg}^{-1}$ instead of $0.015 \text{ dB deg}^{-1}$) typical for tropical rain.

The standard deviation of the estimate of the total span of differential phase $\Delta\Phi_{DP}$ in Eq. (15) is usually of

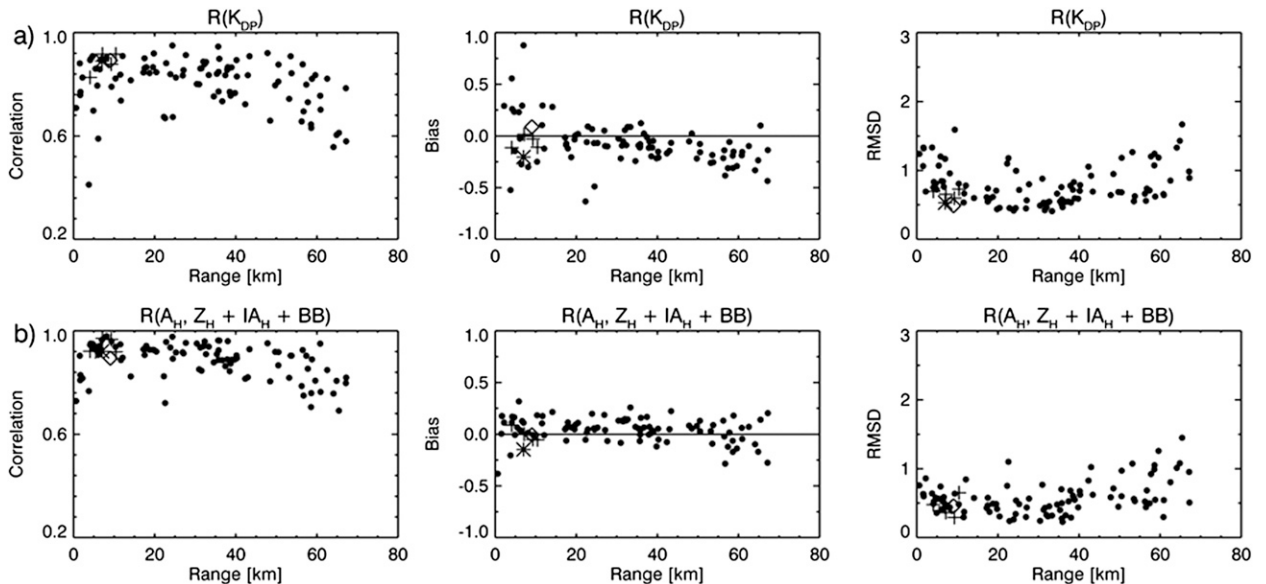


FIG. 12. Correlation coefficients, biases, and rms errors of hourly rainfall estimates from the BoXPol X-band radar using the $R(A)$ and $R(K_{DP})$ algorithms vs range from the radar as revealed from the comparisons with 133 gauges during five months of continuous observations. The $R(A)$ estimate is complemented by the $R(Z)$ estimate (after Z is corrected for attenuation and PBB) if $\Delta\Phi_{DP} < 4^\circ$. Every symbol in the graphs corresponds to the mean value of the metric in a particular range interval.

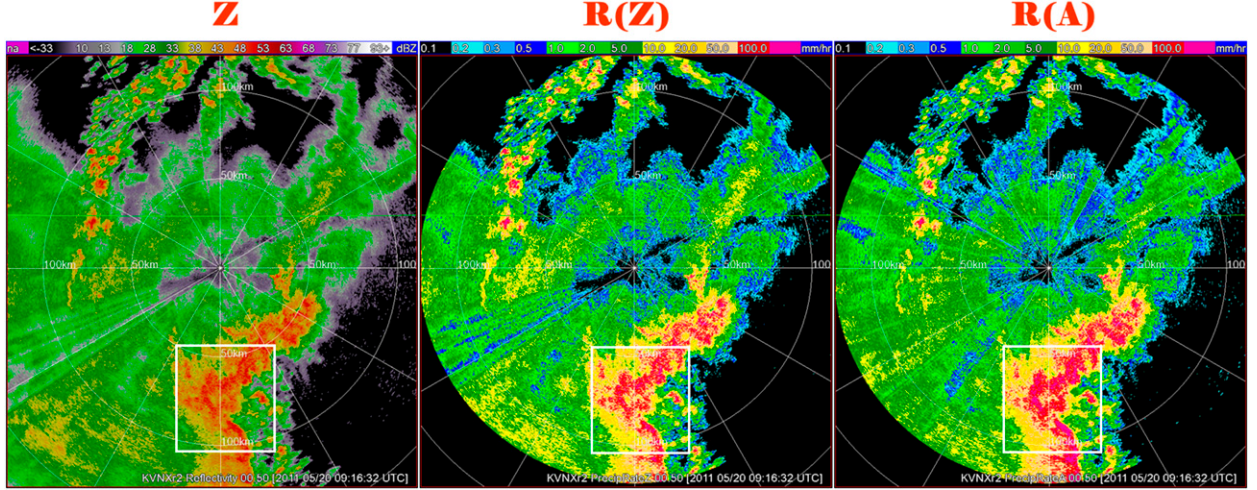


FIG. 13. Maps of Z , $R(Z)$, and $R(A)$ measured by the KVN X WSR-88D radar at 0916 UTC 20 May 2011. The area enclosed in a white square is displayed in Fig. 14.

the order of 1° . Such accuracy is sufficient for a reliable estimation of low $\Delta\Phi_{DP}$ values of few degrees. We have found experimentally that the method yields stable results if $\Delta\Phi_{DP}$ is higher than 4° at X band and 2° – 3° at S band. At radials with lower values of $\Delta\Phi_{DP}$, rain rates are determined using a standard $R(Z)$ relation subjected to attenuation correction.

c. The performance of $R(A)$ in hail

Extensive testing of the $R(A)$ method using multiple WSR-88D radars and various rain events confirms the theoretical prediction that $R(A)$ tends to overestimate rain in areas where rain is mixed with hail. To address this issue, we segment those radials within which hail is

identified and utilize $R(K_{DP})$ in the range gates contaminated with hail. If K_{DP} is less than $0.1^\circ \text{ km}^{-1}$ in the hail area, then the $R(Z)$ relation (with Z capped at 53 dBZ) is used instead of $R(K_{DP})$.

The performance of the original [pure $R(A)$] and the modified [$R(A)$ combined with $R(K_{DP})$ and $R(Z)$] algorithms for a hail-bearing storm observed by the KICT WSR-88D radar on 30 May 2012 is illustrated in Fig. 18. Several strong hail cells passed over the radar coverage area during a 6-h interval. Some hail cells produce really big hailstones with sizes up to 4.5 cm. The unmodified $R(A)$ algorithm clearly overestimates rain totals in the areas of enhanced precipitation where significant amounts of hail fell (Fig. 18a). One of the gauges in the

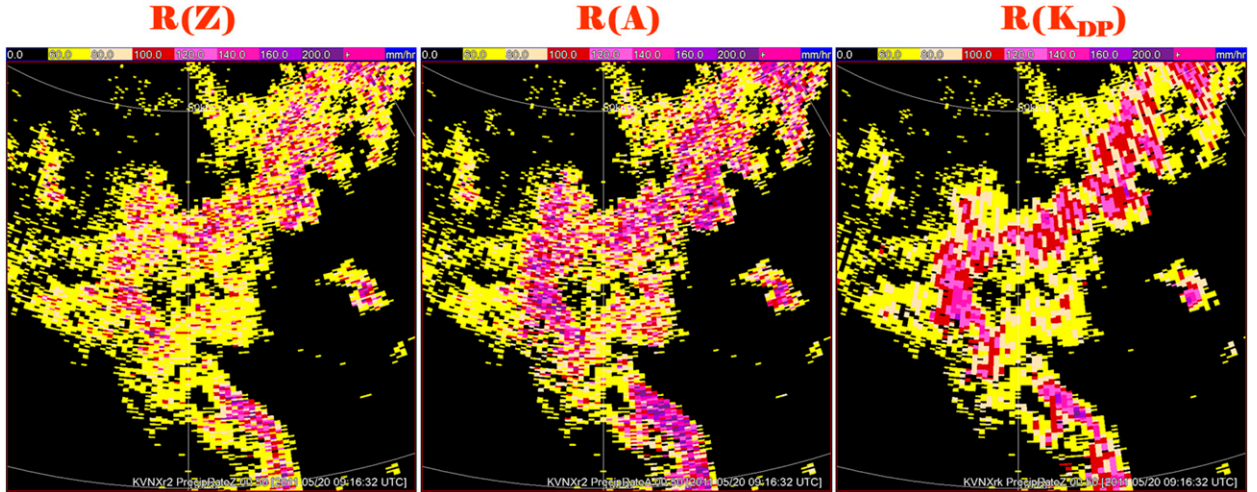


FIG. 14. Comparison of the texture of the fields of $R(Z)$, $R(A)$, and $R(K_{DP})$ measured by the KVN X WSR-88D radar on 20 May 2011 in the area enclosed in a white box in Fig. 13. Only the data with $Z > 45 \text{ dBZ}$ are displayed.

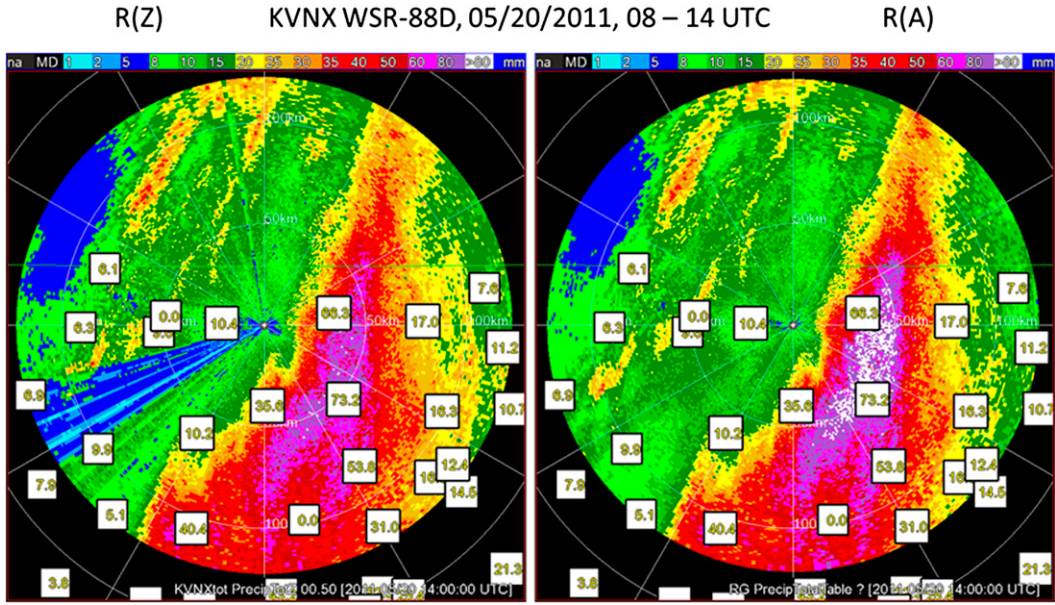


FIG. 15. Maps of 6-h rain total obtained from the KVN WSR-88D radar on 20 May 2011 (0800–1400 UTC) using the $R(Z)$ and $R(A)$ algorithms. Gauge accumulations (mm) are displayed in white squares.

area of high rain totals indicates a 6-h accumulation of 80 mm, whereas the unmodified $R(A)$ algorithm yields about 150–200 mm of rain there. On the other hand, the modified $R(A)$ algorithm that combines $R(A)$, $R(K_{DP})$, and $R(Z)$ produces lower rain totals in areas contaminated by hail (Fig. 18b). The performance of both algorithm versions is better quantified in the bottom panels of Fig. 18, where the scatterplots of 6-h gauge

totals versus their radar estimates are shown. The combined algorithm produces a better agreement of the radar estimate with the gauge.

d. Radar networking

Because the $R(A)$ estimate is immune to radar miscalibration and partial beam blockage, it has benefits for mosaicking rainfall products obtained from neighboring

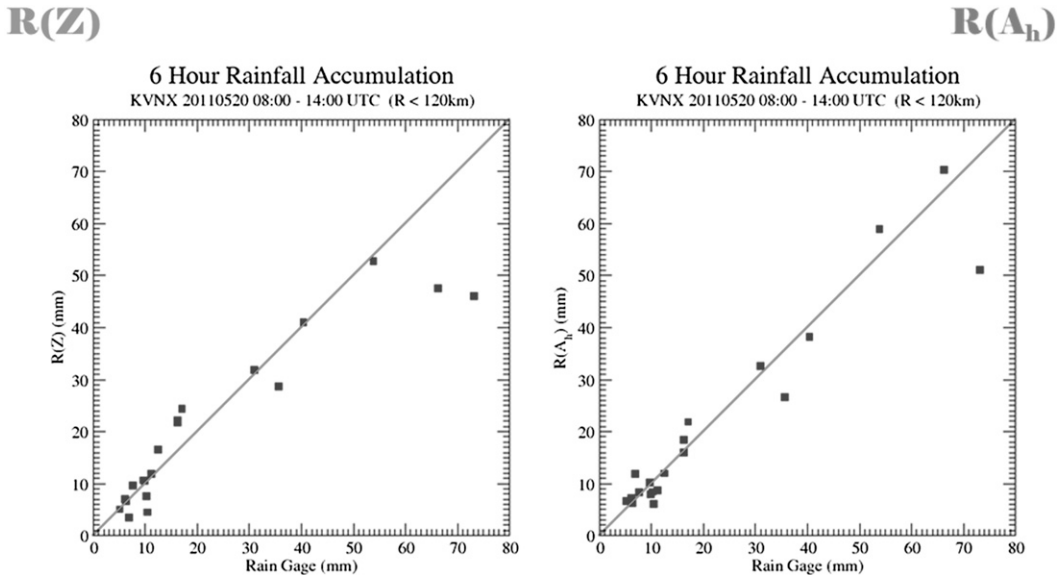


FIG. 16. Scatterplots of 6-h rain total obtained from gauges vs their estimates by the KVN WSR-88D radar on 20 May 2011 using the $R(Z)$ and $R(A)$ algorithms with $\alpha = 0.015 \text{ dB deg}^{-1}$.

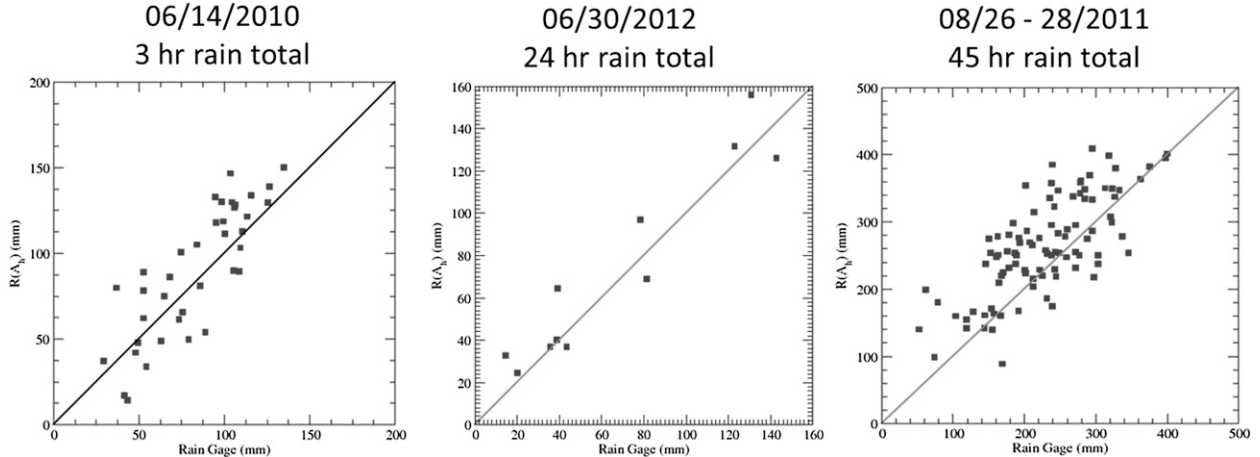


FIG. 17. Scatterplots of rain totals estimated by the $R(A)$ method vs their estimates from rain gauges for three heavy rain events.

radars. In Fig. 19, the standard mosaic rainfall product is obtained by merging the data from the KVN-X and KICT WSR-88D radars. Maps of 8-h rain totals for a rain event on 13 September 2012 are retrieved using the $R(Z)$ and $R(A)$ algorithms (left and right panels, respectively). The estimated $R(Z)$ rainfall amount shows a large discontinuity along the equidistant line between the two radars because the KVN-X radar is about 2 dB “colder” than the KICT radar. The $R(A)$ 8-h rain totals obtained from both radars are much more consistent and there is no discontinuity along the equidistant line except one short segment in the center, probably caused by inadequate second-trip echo mitigation. There is also evidence of excessive ground clutter removal along the zero Doppler velocity iso-dops that causes artificial negative bias in Z along that part of the radial. PBB impacts are better mitigated by the $R(A)$ method but not completely removed because the radar signal can be totally lost in a blocked sector during light rain and the retrieval of specific attenuation is not possible.

The $R(A)$ methodology also allows for seamless mosaics of rain total from radars operating at different wavelengths. Figure 20 illustrates a composite of the 6-h rain total products obtained from the KBUF WSR-88D

radar in Buffalo, New York, and the C-band polarimetric radar in King City, Ontario, Canada, for the rain event on 8 September 2012. The left panel shows a composite plot using rainfall estimates from the $R(Z)$ relation before attenuation correction is performed at C band. The discontinuity in the map of 6-h rain accumulation along the line of equidistant range from the two radars is clearly visible and can be attributed to the Z biases caused by possible radar miscalibration and/or stronger attenuation at C band. This discontinuity becomes less pronounced once the C-band Z is corrected for attenuation using differential phase (middle panel in Fig. 20). However, it is the utilization of the $R(A)$ technique for both radars that results in the seamless map of composite rainfall accumulation (right panel in Fig. 20).

8. Conclusions

Rainfall estimation utilizing specific attenuation A has many advantages compared to algorithms based on Z , Z_{DR} , or K_{DP} . It is least sensitive to DSD variations and immune to radar miscalibration, partial beam blockage, and impacts of wet radomes. In addition, the $R(A)$ estimate has a radial resolution equal to $R(Z)$ and thus

TABLE 3. Bias ratios, FRMSEs, and correlation coefficients of the $R(A)$ estimates of rain totals for four heavy rain events.

Storm date	WSR-88D radar	Accumulation interval (h)	Bias ratio (R/G)	FRMSE (%)	Corr coef
14 Jun 2010	KTLX	3	1.08	26.3	0.836
20 May 2011	KVN-X	6	0.96	26.7	0.958
26–28 Aug 2011	KMHX	45	1.16	29.1	0.730
30 Jun 2012	KDLH	24	1.09	22.4	0.951

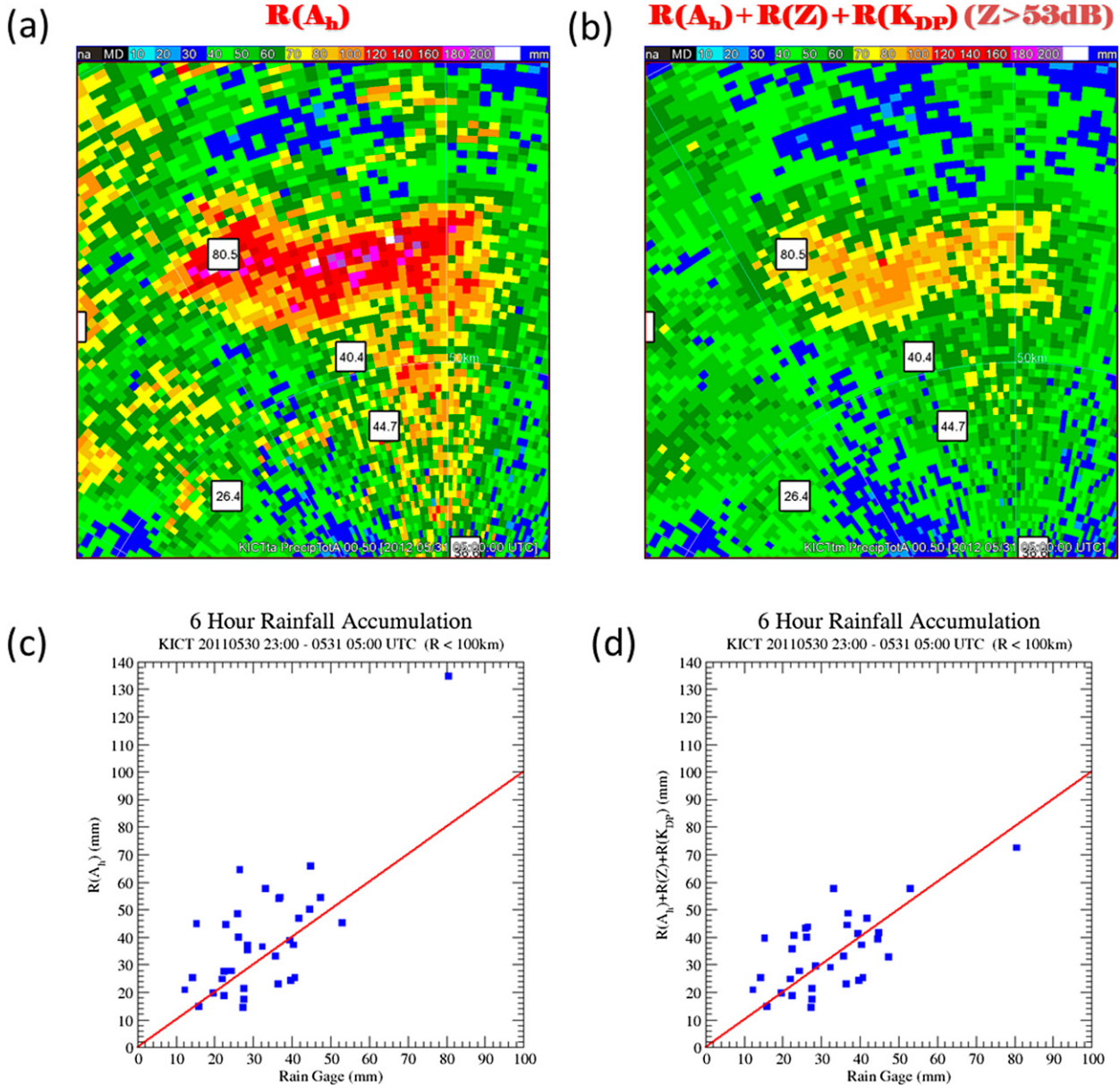


FIG. 18. Maps of 6-h rain accumulation retrieved by the KICT WSR-88D radar for the period from 2300 UTC 30 May 2012 to 0500 UTC 31 May 2012 using (a) the standard $R(A)$ algorithm and (b) the modified algorithm in which $R(A)$ is combined with $R(K_{DP})$ [or $R(Z)$ with Z capped at the 53 dBZ level] in the areas of rain mixed with hail. White boxes indicate 6-h rain totals measured by gauges. Scatterplots of 6-h rain totals from gauges vs their radar estimates obtained with (c) the standard and (d) modified $R(A)$ algorithms.

a better resolution than the $R(K_{DP})$ estimate. The shape of rain cells retrieved by the $R(A)$ algorithm is not distorted compared to $R(Z)$ estimates in contrast to $R(K_{DP})$ estimates. The method is very simple and easy to use, since only the radial profile of attenuated reflectivity and the total span of the differential phase $\Delta\Phi_{DP}$ along the propagation path are required. Robust retrieval of A can be made if $\Delta\Phi_{DP}$ exceeds only 2° – 4° .

The examination of the $R(A)$ performance for convective storms producing heavy rain with significant variability of normalized concentration of raindrops N_w shows that the estimate of specific attenuation A retrieved from the basic ZPHI formula is sufficiently accurate and does not need segmentation of the propagation path, which is required for the classical ZPHI method introduced by Testud et al. (2000). Such segmentation is

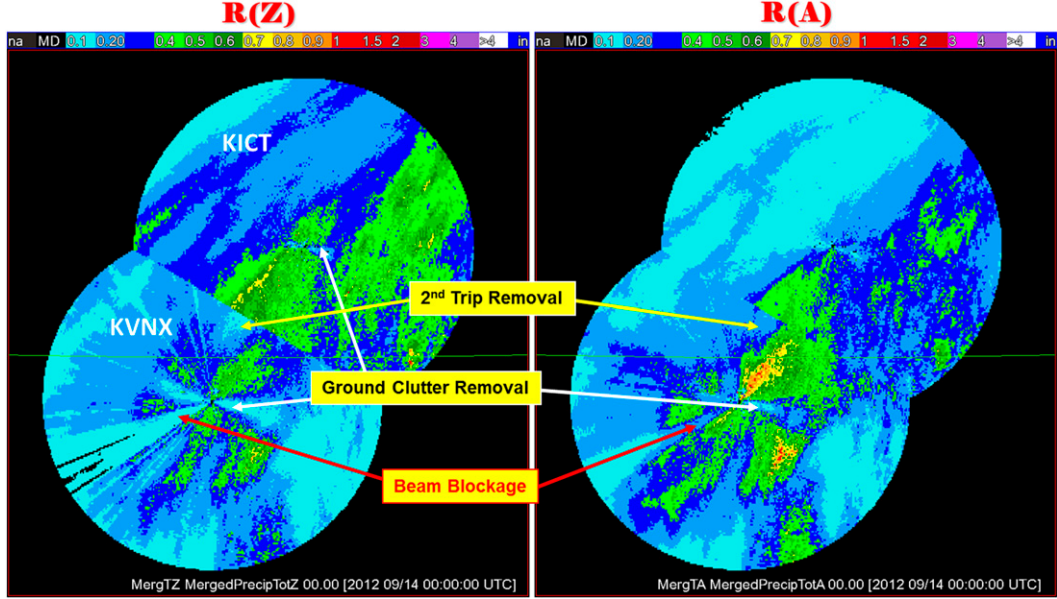


FIG. 19. Composite maps of 8-h rain total obtained from the KVNX and KICT WSR-88D radars using the $R(Z)$ and $R(A)$ relations on 13 Sep 2012.

needed, however, if really strong “hot spots” are identified along the propagation path, which are commonly associated with the presence of hail. The dependence of the retrieved A on temperature and the net ratio $\alpha = A/K_{DP}$ along the ray poses certain problems that can be solved using known vertical profiles of temperature and by optimizing α .

The $R(A)$ method is applicable for all radar wavelengths utilized in radar meteorology including S band,

where attenuation is usually vanishingly small. Polarimetric radar observations at X and S bands confirm that the method is immune to partial beam blockage and radar miscalibration and can be efficient for radar networking. The comparison of rainfall estimates obtained using different radar algorithms with the gauges shows that the $R(A)$ method outperforms others [e.g., $R(K_{DP})$] at X band and demonstrates robust performance at S band.

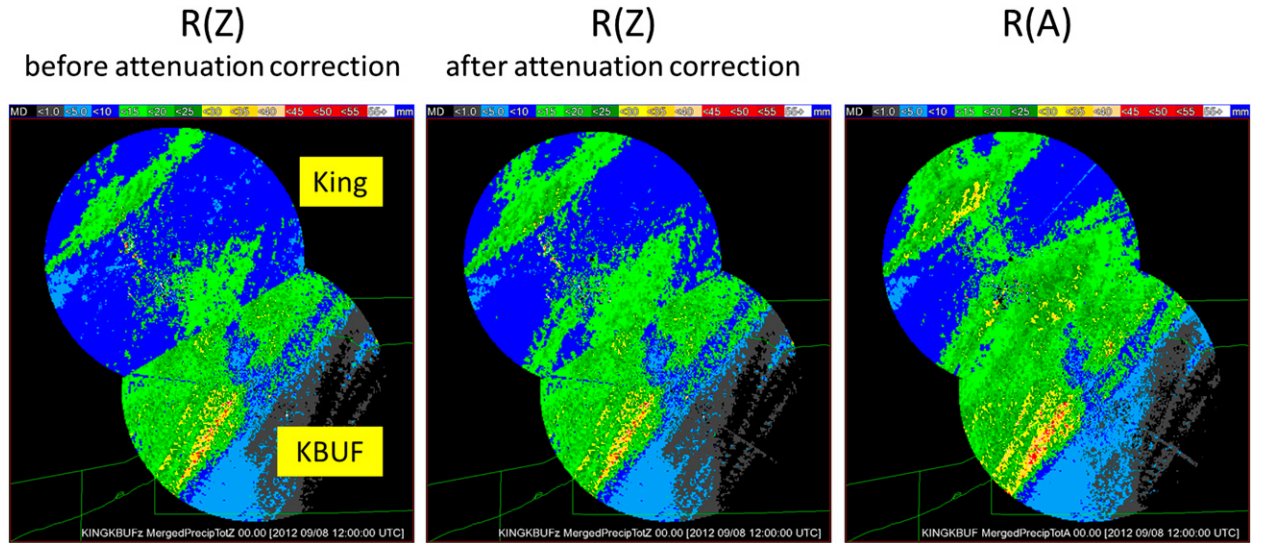


FIG. 20. Composite maps of 6-h rain total obtained from the King City polarimetric C-band radar and KBUF WSR-88D radar using the $R(Z)$ (before and after attenuation correction) and $R(A)$ relations on 8 Sep 2012.

Acknowledgments. Funding for the study was provided by NOAA/Office of Oceanic and Atmospheric Research under NOAA–University of Oklahoma Cooperative Agreement NA11OAR4320072, U.S. Department of Commerce, and by the U.S. National Weather Service, Federal Aviation Administration, and U.S. Department of Defense program for modernization of NEXRAD radars. Funding for the study was also provided by the Deutsche Forschungsgemeinschaft (DFG) in the framework of the Collaborative Research Center TR32, and by the OASE branch of the Hans-Ertel-Zentrum für Wetterforschung (HErZ). We also acknowledge funding of the Jülich polarimetric X-band radar by the TERENO program of the Helmholtz Association. Our special thanks are extended to Dr. David Hudak from Environment Canada for providing the King City C-band radar data.

REFERENCES

- Atlas, D., and C. W. Ulbrich, 1977: Path- and area-integrated rainfall measurement by microwave attenuation in the 1–3 cm band. *J. Appl. Meteor.*, **16**, 1322–1331.
- Brandes, E., G. Zhang, and J. Vivekanandan, 2002: Experiments in rainfall estimation with polarimetric radar in a subtropical environment. *J. Appl. Meteor.*, **41**, 674–685.
- Bringi, V. N., V. Chandrasekar, N. Balakrishnan, and D. S. Zrnić, 1990: An examination of propagation effects in rainfall on polarimetric variables at microwave frequencies. *J. Atmos. Oceanic Technol.*, **7**, 829–840.
- , T. D. Keenan, and V. Chandrasekar, 2001: Correcting C-band radar reflectivity and differential reflectivity data for rain attenuation: A self-consistent method with constraints. *IEEE Trans. Geosci. Remote Sens.*, **39**, 1906–1915.
- , V. Chandrasekar, J. Hubbert, E. Gorgucci, W. Randeu, and M. Schoenhuber, 2003: Raindrop size distribution in different climatic regimes from disdrometer and dual-polarized radar analysis. *J. Atmos. Sci.*, **60**, 354–365.
- Cifelli, R., V. Chandrasekar, S. Lim, P. Kennedy, Y. Wang, and S. Rutledge, 2011: A new dual-polarization radar rainfall algorithm: Application in Colorado precipitation events. *J. Atmos. Oceanic Technol.*, **28**, 352–364.
- Fabry, F., 2001: Using radars as radiometers: Promises and pitfalls. Preprints, *30th Conf. on Radar Meteorology*, Munich, Germany, Amer. Meteor. Soc., P5.1. [Available online at https://ams.confex.com/ams/30radar/techprogram/paper_21576.htm.]
- Figueras i Ventura, J., A.-A. Baumahmoud, B. Fradon, P. Dupuy, and P. Tabary, 2012: Long-term monitoring of French polarimetric radar data quality and evaluation of several polarimetric quantitative precipitation estimators in ideal conditions for operational implementation at C-band. *Quart. J. Roy. Meteor. Soc.*, **138**, 2212–2228.
- Giangrande, S., and A. Ryzhkov, 2008: Estimation of rainfall based on the results of polarimetric echo classification. *J. Appl. Meteor.*, **47**, 2445–2462.
- Hitschfeld, W., and J. Bordan, 1954: Errors inherent in the radar measurement of rainfall at attenuating wavelengths. *J. Meteor.*, **11**, 58–67.
- Iguchi, T., and R. Meneghini, 1994: Intercomparison of single-frequency methods for retrieving a vertical rain profile from airborne or spaceborne radar data. *J. Atmos. Oceanic Technol.*, **11**, 1507–1516.
- Illingworth, A. J., and R. J. Thompson, 2005: The estimation of moderate rain rates with operational polarization radar. Preprints, *32nd Conf. on Radar Meteorology*, Albuquerque, NM, Amer. Meteor. Soc., P9R.1. [Available online at https://ams.confex.com/ams/32Rad11Meso/techprogram/paper_96204.htm.]
- , —, T. Darlington, and J. Owens, 2011: Emission: A new technique to correct rainfall estimates for attenuation. Preprints, *35th Conf. on Radar Meteorology*, Pittsburgh, PA, Amer. Meteor. Soc., 19B.1. [Available online at <http://ams.confex.com/ams/35Radar/flvgateway.cgi/id/18670?recordingid=18670>.]
- Le Bouar, E., and J. Testud, 2001: A new scheme to estimate rain rate from an S-band polarimetric radar, immune with respect to DSD variability and radar calibration error. Preprints, *30th Int. Conf. Radar Meteorology*, Munich, Germany, Amer. Meteor. Soc., P16.11. [Available online at https://ams.confex.com/ams/30radar/techprogram/paper_21522.htm.]
- , —, and T. D. Keenan, 2001: Validation of the rain profiling algorithm “ZPHI” from the C-band polarimetric weather radar in Darwin. *J. Atmos. Oceanic Technol.*, **18**, 1819–1837.
- Maesaka, T., K. Iwanami, and M. Maki, 2012: Non-negative K_{DP} estimation by monotone increasing Φ_{DP} assumption below melting layer. *Extended Abstracts, Seventh European Conf. on Radar in Meteorology and Hydrology*, Toulouse, France, Météo-France, 26 QPE. [Available online at http://www.meteo.fr/cic/meetings/2012/ERAD/ERAD2012_programme.pdf.]
- Marzoug, M., and P. Amayenc, 1994: A class of single- and dual-frequency algorithms for rain-rate profiling from a spaceborne radar. Part I: Principle and tests from numerical simulations. *J. Atmos. Oceanic Technol.*, **11**, 1480–1506.
- Matrosov, S., 2005: Attenuation-based estimates of rainfall rates aloft with vertically pointing Ka-band radars. *J. Atmos. Oceanic Technol.*, **22**, 43–54.
- Meneghini, R., and K. Nakamura, 1990: Range profiling of the rain rate by an airborne weather radar. *Remote Sens. Environ.*, **31**, 193–209.
- Moupfouma, F., 1984: Improvement of rain attenuation prediction method for terrestrial microwave links. *IEEE Trans. Antennas Propag.*, **32**, 1368–1372.
- Otto, T., and H. Russchenberg, 2011: Estimation of specific differential phase and differential backscatter phase from polarimetric weather radar measurements of rain. *IEEE Geosci. Remote Sens. Lett.*, **8**, 988–992.
- Overeem, A., H. Leijnse, and R. Uijlenhoet, 2011: Measuring urban rainfall using microwave links from commercial cellular communication networks. *Water Resour. Res.*, **47**, W12505, doi:10.1029/2010WR010350.
- Park, S.-G., V. Bringi, V. Chandrasekar, M. Maki, and K. Iwanami, 2005: Correction of radar reflectivity and differential reflectivity for rain attenuation at X band. Part II: Evaluation and application. *J. Atmos. Oceanic Technol.*, **22**, 1633–1655.
- Ryzhkov, A. V., 2007: The impact of beam broadening on the quality of radar polarimetric data. *J. Atmos. Oceanic Technol.*, **24**, 729–744.
- , S. Ganson, A. Khain, M. Pinsky, and A. Pokrovsky, 2009: Polarimetric characteristics of melting hail at S and C bands. Preprints, *34th Conf. on Radar Meteorology*, Williamsburg, VA, Amer. Meteor. Soc., 4A.6. [Available online at <http://ams.confex.com/ams/pdfpapers/155571.pdf>.]
- , —, M. Kumjian, and R. Kaltenboeck, 2012: Polarimetric characteristics of dry and melting hail at different radar

- wavelengths. *Extended Abstracts, Seventh European Conf. on Radar in Meteorology and Hydrology*, Toulouse, France, Météo-France, 2.1. [Available online at <http://www.meteo.fr/cic/meetings/2012/ERAD/presentations/monday/2-1.pdf>.]
- Schuur, T. J., A. V. Ryzhkov, D. S. Zrnić, and M. Schönhuber, 2001: Drop size distributions measured by a 2D video disdrometer: Comparison with dual-polarization radar data. *J. Appl. Meteor.*, **40**, 1019–1034.
- , —, and D. R. Clabo, 2005: Climatological analysis of DSDs in Oklahoma as revealed by 2D-video disdrometer and polarimetric WSR-88D. Preprints, 32nd Conf. on Radar Meteorology, Albuquerque, NM, Amer. Meteor. Soc., 15R.4. [Available online at https://ams.confex.com/ams/32Rad11Meso/techprogram/paper_95995.htm.]
- Tabary, P., A.-A. Boumahmoud, H. Andrieu, R. J. Thompson, A. J. Illingworth, E. LeBouar, and J. Testud, 2011: Evaluation of two “integrated” polarimetric quantitative precipitation estimation (QPE) algorithms at C-band. *J. Hydrol.*, **405**, 248–260.
- Testud, J., E. Le Bouar, E. Obligis, and M. Ali-Mehenni, 2000: The rain profiling algorithm applied to polarimetric weather radar. *J. Atmos. Oceanic Technol.*, **17**, 332–356.
- , S. Oury, R. Black, P. Amayenc, and X. Dou, 2001: The concept of “normalized” distribution to describe raindrop spectra: A tool for cloud physics and cloud remote sensing. *J. Appl. Meteor.*, **40**, 1118–1140.
- Trömel, S., M. R. Kumjian, A. V. Ryzhkov, C. Simmer, and M. Diederich, 2013: Backscatter differential phase—Estimation and variability. *J. Appl. Meteor. Climatol.*, **52**, 2529–2548.
- Vulpiani, G., M. Montopoli, L. Delli Passeri, A. Giola, P. Giordano, and F. Marzano, 2012: On the use of dual-polarized C-band radar for operational rainfall retrieval in mountainous area. *J. Appl. Meteor. Climatol.*, **51**, 405–425.
- Wang, Y., and V. Chandrasekar, 2009: Algorithm for estimation of the specific differential phase. *J. Atmos. Oceanic Technol.*, **26**, 2565–2578.